


Article

Processes and Conditions of the Origin for Fe³⁺-Bearing Magnesiowürstite under Lithospheric Mantle Pressures and Temperatures

Yuliya Bataleva ^{1,*} , Yuri Palyanov ^{1,2}, Yuri Borzdov ¹ and Oleg Bayukov ³¹ Sobolev Institute of Geology and Mineralogy, Siberian Branch of Russian Academy of Sciences, Koptyug ave 3, 630090 Novosibirsk, Russia² Department of Geology and Geophysics, Novosibirsk State University, Pirogova str 2, 630090 Novosibirsk, Russia³ Kirensky Institute of Physics, Siberian Branch of Russian Academy of Sciences, Akademgorodok 50, bld. 38, 660036 Krasnoyarsk, Russia

* Correspondence: bataleva@igm.nsc.ru; Tel.: +7-383-330-75-01

Received: 16 June 2019; Accepted: 30 July 2019; Published: 1 August 2019



Abstract: An experimental study, implicated in the revealing of the conditions for the origin for Fe³⁺-bearing magnesiowürstite in the lithospheric mantle, was performed using Mössbauer spectroscopy of pre-synthesized samples. Experiments were carried out using a multi-anvil high-pressure split-sphere apparatus at 6.3–7.5 GPa, in the range of 1100–1650 °C in carbonate-metal, carbonate-oxide-metal, carbonate-oxide, carbide-oxide and carbonate-metal- sulphur systems. In three experimental series, oxygen fugacity gradient in the samples was created, which enabled the study of the processes of magnesiowürstite formation under oxidizing and reducing conditions ($\Delta \log fO_2$ (FMQ) values from −1 to −5). It was established that Fe³⁺-bearing magnesiowürstite can form both in assemblage with oxidized phases, such as carbonate or with reduced ones—metal, carbides, sulphides, graphite and diamond. According to the Mössbauer spectroscopy, the composition of synthesized magnesiowürstite varied within a range of Fe³⁺/ΣFe values from 0 to 0.3, with IV and VI coordination of Fe³⁺ depending on P, T, fO_2 , x-parameters. It was established that Fe³⁺-bearing magnesiowürstite formation processes under upper mantle P,T-conditions include redox reactions, with magnesiowürstite being (1) reductant or (2) product of interaction, (3) crystallization processes of magnesiowürstite from an oxidized melt, where magnesiowürstite acts as a sink for ferric iron and (4) iron disproportionation.

Keywords: Fe³⁺-bearing magnesiowürstite; mantle oxides; experimental modeling; high-pressure experiment; redox reactions; lithospheric mantle; diamond; graphite

1. Introduction

1.1. Distribution of Mg, Fe-Oxides in the Earth's Interior

According to experimental and theoretical data, ferropericlase and magnesiowürstite are considered the most abundant oxide minerals in the Earth's interior; they are thought to comprise approximately 16–20 wt.% of the lower mantle [1–10]. The presence of ferropericlase in the lower mantle is caused by the decomposition of transition zone minerals to Mg–Si perovskite and MgO at the 650-km discontinuity [11,12]. However, a distribution area of Mg,Fe-oxides in the Earth's interior is not limited to the lower mantle. Minor amounts of ferropericlase and magnesiowürstite occur in the Earth's crust, in the rocks altered in high-temperature contact metamorphic processes. The upper mantle occurrences of ferropericlase were proposed to exist after comprehensive study and criticism of “lower mantle”

parageneses of some inclusions in diamonds from São Luiz (Brazil) [13,14]. In the early 2000s this idea was developed and it was shown that (1) ferropericlase may form as inclusions in diamonds at upper mantle conditions, provided that the Si activity was low enough [15] and (2) ferropericlase exists in the upper mantle in regions with low silica activity, such as carbonated dunite or stalled and degassed carbonatitic melts [16]. Despite these ideas, most of the modern studies devoted to the investigation of Mg,Fe-oxides in the Earth's mantle are limited to the lower mantle conditions.

1.2. Crustal Structure and Composition of Mg,Fe-Oxides in the Mantle

Studies on crystal structure and phase transitions demonstrate that MgO-FeO forms a complete solid solution series with a gradual compositional transition between the end-member periclase and wüstite in the cubic crystal structure B1 (NaCl type with $Z = 4$) with space group $Fm\bar{3}m$, in which end-members differ only in crystal parameters. For intermediate compositions, the structure consists of interpenetrating face-centred-cubic lattices producing alternating Mg^{2+}/Fe^{2+} cations and O^{2-} anions [17,18]. Pure periclase (MgO) was found to be stable with the B1 structure to at least 227–250 GPa, that is, to pressures in the bottom of the lower mantle [19,20]. By contrast, wüstite (FeO) experiences a number of phase transitions under high-pressure and high-temperature conditions, which are shown in Figure 1.

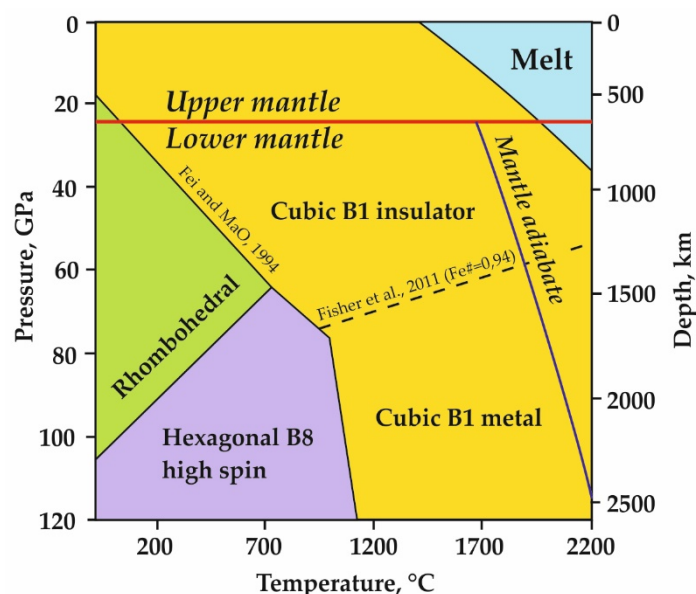


Figure 1. Phase diagram for wüstite at high pressures and temperatures, after [18]. Data from References [7,21–28]. Mantle adiabat after [29].

The most reliable sources of information on magnesiowüstite and ferropericlase compositions under upper and lower mantle conditions are the inclusions of these minerals in diamonds. Studies of natural diamonds from kimberlite pipes in Canada, Brazil and Guinea demonstrate that (Mg,Fe)O crystals are present in 50–56% of inclusions [10,30–34]. Natural ferropericlase and magnesiowüstite series from diamond inclusions occupies a composition range, almost reaching both end-members [18]; however, there are different compositional trends for these Fe,Mg-oxides originating from lower and upper mantle. More specifically, the ferruginosity ($Fe\#$, $Fe/(Fe+Mg)$ ratio) of ferropericlase inclusions in diamonds from the lower mantle is about 0.10–0.65 [10,30,34–38] and very rarely it has almost wüstite-endmember stoichiometry with $Fe\#$ of 0.84 [39]. Magnesiowüstite from the upper mantle assemblages is usually characterized by $Fe\#$ from 0.5 to 1 [35,40,41].

The distribution regularities of ferric ions in the structure of upper- and lower mantle originated ferropericlase and magnesiowüstite were revealed. Multi-method analysis of ferropericlase grains from inclusions in super-deep diamonds from the Juina kimberlites [18,42] demonstrated the inhomogeneous

distribution of Fe^{3+} and its concentrations in iron-rich, nanosize magnesioferrite-like clusters. It was established that $\text{Fe}^{3+}/\Sigma\text{Fe}$ ratios in ferropericlasite were much lower than in the FeO-rich magnesio-wüstite and wüstite samples [43]. Depending on the method, $\text{Fe}^{3+}/\Sigma\text{Fe}$ ratios in ferropericlasite in diamond inclusions were estimated at approximately 0–7% [36,44], 3–9 % [45], 8–12 % [42,46]. Besides the studies on incorporation of ferric iron in ferropericlasite and magnesio-wüstite, there are theoretical studies predicting the metallization of FeO (B1 structure type) at high pressures [47–49]. Recent experiments demonstrated that B1-structured FeO metallizes at around 70 GPa and ~1600 °C without phase transition or any structure changes [50]. The mechanism of incorporation of Fe^{3+} or metallization of ferropericlasite and magnesio-wüstite affects the iron atomic diffusion and electrical conductivity, as well as its rheological properties [27,51–53].

1.3. Modern Concepts on the Fe^{3+} -Bearing Magnesio-wüstite Formation in the Upper Mantle

Despite that magnesio-wüstite and ferropericlasite are predominantly formed in the lower mantle, processes of their crystallization can occur in the upper mantle as well. Since concentration of the ferric iron in (Mg,Fe)O is strongly dependent on variations in the redox conditions of a host upper mantle domain [32,36,54–56], the presence of Fe^{3+} -bearing magnesio-wüstite can indicate certain redox reactions. For example, the formation of oxidized mantle domains is usually associated with subduction and reflected by the presence of carbonate minerals [57–61] as well as Fe^{3+} -bearing magnesio-wüstite. It is proposed that formation of Fe^{3+} -bearing magnesio-wüstite can occur as a result of the redox reactions of magnesio-wüstite with carbonates, CO_2 or carbonate-bearing melts, according to the following simplified reactions: $4\text{FeO} + \text{CO}_2 \rightarrow 2\text{Fe}_2\text{O}_3 + \text{C}^0$ [60] and $6\text{FeO} + \text{CO}_2 \rightarrow 2\text{Fe}_3\text{O}_4 + \text{C}^0$ [62].

However, results of our previous experimental studies, supported by Mössbauer spectroscopy data, demonstrate that formation of Fe^{3+} -bearing magnesio-wüstite in assemblage with elemental carbon (graphite or diamond) can occur both under oxidizing and reducing conditions. More specifically, experimental modelling of carbonate-metal [63], carbonate-oxide-metal [64], carbonate-oxide [65], carbide-oxide [66] and carbonate-metal-sulphur [67,68] interactions shows very different scenarios of the formation of this assemblage. However, these studies were not aimed directly at the modeling of formation processes of the Fe^{3+} -bearing magnesio-wüstite. Thus, it is very relevant to investigate all complexity of these processes in various experimental series and propose models of the formation of Fe^{3+} -bearing magnesio-wüstite + graphite/diamond assemblage under the upper mantle P,T conditions. The purpose of this study is an experimental modelling of the conditions for the formation of the Fe^{3+} -bearing magnesio-wüstite + graphite/diamond assemblage in carbonate-metal, carbonate-oxide-metal, carbonate-oxide, carbide-oxide and carbonate-sulphur-metal systems using the Mössbauer spectroscopy.

2. Materials and Methods

Experimental studies devoted to the revealing of the formation processes of Fe^{3+} -bearing magnesio-wüstite and wüstite (in an assemblage with graphite or diamond) at P, T, $f\text{O}_2$ and environment composition parameters typical of the lithospheric mantle were carried out using a multi-anvil high-pressure split-sphere apparatus (BARS) [69]. The methodological features of the high-pressure cell design and calibration data were published elsewhere [70,71]. Fe^{3+} -bearing magnesio-wüstite was synthesized in carbonate-iron ((Mg,Ca) CO_3 - Fe^0) [63], carbonate-iron-sulphur ((Mg,Ca) CO_3 - Fe^0 -S 0) [67,68], carbide-oxide (Fe_3C - Fe_2O_3) [66], carbonate-oxide ((Mg,Ca) CO_3 - SiO_2 - Al_2O_3 -FeO) [65] and carbonate-oxide-metal ((Mg,Ca) CO_3 - SiO_2 - Al_2O_3 - Fe^0) [64] systems at pressures of 6.3–7.5 GPa and in a temperature range of 900–1600 °C, with a duration of 18–60 h. The experimental parameters, system compositions, final phase assemblages and magnesio-wüstite composition are given in Tables 1 and 2. Experiments were performed using two different methodological approaches and assembly designs, the so-called “sandwich-type” and “mixture-type.”

Table 1. Summary of the results of experiments in the carbonate-metal, carbonate-metal-sulphur, carbide-oxide, carbonate-oxide, carbonate-oxide-metal systems.

Run N	P, GPa	T, °C	t, h	Sample Zone	Phase Assemblage	Magnesiowüstite and Wüstite Composition
Carbonate-metal system						
1541	7.5	1000	60	Reduced	Mws (17) + Coh (81) + Gr (2)	$\text{Mg}_{0.12-0.35}\text{Fe}^{2+}_{0.65-0.88}\text{O}$
				Oxidized	Mws (62) + Marg (36) + Gr (2)	$\text{Mg}_{0.38}\text{Fe}^{2+}_{0.42-0.57}\text{Fe}^{3+}_{0.02-0.15}\text{O}$
1525	7.5	1400	60	Reduced	Mws (57) + L _{carb} (37) + Gr (3) + Dm (3)	$\text{Mg}_{0.37}\text{Fe}_{0.60}\text{Fe}^{3+}_{0.03}\text{O}$
				Oxidized	Mws (34) + L _{carb} (25) + Fms (25) + Gr (3) + Dm (3)	$\text{Mg}_{0.38}\text{Fe}^{2+}_{0.55}\text{Fe}^{3+}_{0.06}\text{O}$
1250	6.5	1450	20	Reduced	Mws (61) + Coh (37) + Dm (2)	$\text{Mg}_{0.27-0.30}\text{Fe}^{2+}_{0.62-0.68}\text{Fe}^{3+}_{0.05}\text{O}$
				Oxidized	Mws (15) + L _{carb} (82) + Gr (2) + Dm (1)	$\text{Mg}_{0.33-0.39}\text{Fe}^{2+}_{0.42-0.44}\text{Fe}^{3+}_{0.19}\text{O}$
1515	7.5	1550	20	Reduced	Mws (80) + L _{carb} (12) + Gr (6) + Dm (2)	$\text{Mg}_{0.42}\text{Fe}^{2+}_{0.51}\text{Fe}^{3+}_{0.05}\text{O}$
				Oxidized	Mws (45) + L _{carb} (15) + Fms (36) + Gr (2) + Dm (2)	$\text{Mg}_{0.44}\text{Fe}^{2+}_{0.51}\text{Fe}^{3+}_{0.05}\text{O}$
Carbonate-oxide-metal system						
1287	6.3	1250	20	Reduced	Mws (60) + Coh (8) + Gr (2) + Grt (30)	$\text{Mg}_{0.17}\text{Fe}^{2+}_{0.76}\text{Fe}^{3+}_{0.07}\text{O}$
				Oxidized	Mws (56) + Grt (28) + Ol (8) + Gr (2) + Carb (6)	$\text{Mg}_{0.19}\text{Fe}^{2+}_{0.74}\text{Fe}^{3+}_{0.07}\text{O}$
1250-2	6.3	1450	20	Reduced	Mws (60) + Coh (2) + Gr (4) + Grt (34)	$\text{Mg}_{0.24}\text{Fe}^{2+}_{0.69}\text{Fe}^{3+}_{0.07}\text{O}$
Carbonate-oxide system						
1289	6.3	1150	20	Reduced	Mws (100)	$\text{Mg}_{0.01}\text{Fe}^{2+}_{0.95}\text{Fe}^{3+}_{0.04}\text{O}$
1287-2	6.3	1250	20	Reduced	Mws (100)	$\text{Mg}_{0.12}\text{Fe}^{2+}_{0.80}\text{Fe}^{3+}_{0.08}\text{O}$
1283	6.3	1350	20	Reduced	Mws (100)	$\text{Mg}_{0.13}\text{Fe}^{2+}_{0.73}\text{Fe}^{3+}_{0.14}\text{O}$
Carbide-oxide system						
1623-A4	6.3	900	18	n/a	Ws (93) + Gr (1) + Coh (5)	$\text{Fe}^{2+}_{0.96}\text{Fe}^{3+}_{0.04}\text{O}$
1620-A4	6.3	1100	18	n/a	Ws (93) + Gr (1) + Coh (5)	$\text{Fe}^{2+}_{0.96}\text{Fe}^{3+}_{0.04}\text{O}$
1618-A4	6.3	1400	18	n/a	Ws (93) + Gr (1) + L _{Fe-C} (5) + DG	$\text{Fe}^{2+}_{0.96}\text{Fe}^{3+}_{0.04}\text{O}$
1602-A4	6.3	1600	18	n/a	Ws (93) + Gr (1) + L _{Fe-C} (5) + DG	$\text{Fe}^{2+}_{0.96}\text{Fe}^{3+}_{0.04}\text{O}$
Carbonate-metal-sulphur system						
MSC-23	6.3	900	18	n/a	Po (16) + Mws (22) + Coh (6) + Carb (55) + Gr (1)	$\text{Mg}_{0.32-0.37}\text{Fe}^{2+}_{0.58-0.63}\text{Fe}^{3+}_{0.04}\text{Ca}_{0.02}\text{O}$
MSC-20	6.3	1200	18	n/a	Mws (36) + Po (63) + Gr (1)	$\text{Mg}_{0.29-0.30}\text{Fe}^{2+}_{0.58}\text{Fe}^{3+}_{0.05}\text{Ca}_{0.08}\text{O}$
MSC-18	6.3	1400	18	n/a	Mws (58) + Gr (2) + L _{Fe-S-C} (16) + L _{Fe-S-O} (24)	$\text{Mg}_{0.34}\text{Fe}^{2+}_{0.63}\text{Fe}^{3+}_{0.03}\text{O}$
						$\text{Mg}_{0.44}\text{Fe}_{0.51}\text{Ca}_{0.06}\text{O}$
MSC-02	6.3	1600	18	n/a	Mws (58) + Gr (2) + L _{Fe-S-C} (16) + L _{Fe-S-O} (24)	$\text{Mg}_{0.17}\text{Fe}^{2+}_{0.76}\text{Fe}^{3+}_{0.07}\text{O}$

Mws: magnesiowüstite, Ws: wüstite, Coh: cohenite, Marg: magnesioaragonite, Gr: graphite, Dm: spontaneous diamond, DG: diamond growth on seeds, Carb: carbonate, Po: pyrrhotite, Grt: garnet, Ol: olivine, L_{carb}: predominantly carbonate melt, L_{Fe-S-C}: Fe-S-C melt, L_{Fe-S-O}: Fe-S-O melt, L_{Fe-C}: Fe-C melt; Numbers in parenthesis are weight proportions of final phases in each zone.

Table 2. Representative composition of magnesiowüstite according to the microprobe analysis.

Run N	P, GPa	T, °C	t, h	Sample Zone	Phase	Mass Concentrations, wt. %			
						FeO + Fe ₂ O ₃ *	MgO	CaO	Total
Carbonate-metal system									
1541	7.5	1000	60	Reduced	Mws	77.1	22.6	0.1	99.8
						88.0	13.0	-	101.0
						93.5	7.0	-	100.5
1525	7.5	1400	60	Oxidized	Mws	74.9	25.1	0.2	100.1
				Reduced	Mws	74.2	24.5	0.1	99.0
				Oxidized	Mws	74.3	25.5	0.2	100.0
1250	6.5	1450	20	Reduced	Mws	79.9	19.5	0.5	99.9
				Oxidized	Mws	82.4	16.7	0.4	99.6
						72.3	25.3	-	99.9
1515	7.5	1550	20	Reduced	Mws	73.6	21.3	4.4	99.4
				Oxidized	Mws	71.2	28.5	-	99.7
						69.7	30.1	0.1	99.8
Carbonate-oxide-metal system									
1287	6.3	1250	20	Reduced	Mws	88.9	10.3	-	99.2
				Oxidized	Mws	87.7	11.8	-	99.5
1250-2	6.3	1450	20	Reduced	Mws	85.0	14.6	-	99.6
Carbonate-oxide-metal system									
1289	6.3	1150	20	Reduced	Mws	99.3	0.6	-	99.9
1287-2	6.3	1250	20	Reduced	Mws	93.9	6.9	-	100.9
1283	6.3	1350	20	Reduced	Mws	91.7	7.5	-	99.2
Carbonate-metal-sulphur system									
MSC-23	6.3	900	18	n/a	Mws	77.2	20.7	1.8	99.8
MSC-20	6.3	1200	18	n/a	Mws	76.6	20.2	2.6	99.4
MSC-18	6.3	1400	18	n/a	Mws	76.8	22.7	0.1	99.6
MSC-02	6.3	1600	18	n/a	Mws _{center}	63.3	30.8	5.6	99.0
					Mws _{rim}	89.6	10.1	-	99.7

*: total amount of iron oxides; Mws: magnesiowüstite.

2.1. Methodical Approach for “Sandwich-Type” Experiments

Experiments in the carbonate-iron, carbonate-oxide and carbonate-oxide-metal systems were performed using a special technique that was based on a redox gradient creation by separating the volume of an ampoule into outer (carbonate or carbonate-oxide (oxidized)) and inner (iron concentrator (reduced)) parts (e.g., Figure 2a). This “sandwich” assembly design provides conditions for diamond- and graphite-producing redox reactions of carbonates, CO₂ fluids or carbonate-bearing melts with metallic iron or wüstite at mantle P,T parameters. Natural magnesite and dolomite (<0.5 wt.% of impurities; Satka deposit, Urals, Russia), as well as synthetic SiO₂, Al₂O₃, Fe⁰ and Fe₂O₃ (<0.01 wt.% of impurities), were used as starting reagents. In experiments in the carbonate-iron system, a carbonate container made from a magnesite-dolomite mixture was placed in a Pt capsule (6 or 10 mm in diameter, at 7.5 and 6.5 GPa, respectively). A pellet of pressed iron was mounted in the center of the carbonate container. In experiments in carbonate-oxide and carbonate-oxide-metal systems, a 10 mm Pt capsule contained a pre-pressed mixture of SiO₂ (101.2 mg), Al₂O₃ (56.8 mg), MgCO₃ (106.4 mg) and CaMg(CO₃)₂ (35.5 mg) powders in the form of a container. Metallic iron or wüstite (150 mg) in the form of a “tablet” was placed in the center of this container. After filling the capsule, it was closed and arc welded. The final capsule height varied from 3.5 to 4.0 mm. This arrangement of system components in a Pt capsule enabled investigation of mineral formation processes in iron-bearing systems with involvement of fluids and melts, minimize interactions between the Pt and Fe-bearing phases. After experiments, the material of Pt capsule walls was analysed by microprobe analysis. According to

the obtained data, the iron content in Pt did not exceed 0.5 wt.%. The details of this methodological approach are described in References [63–65].

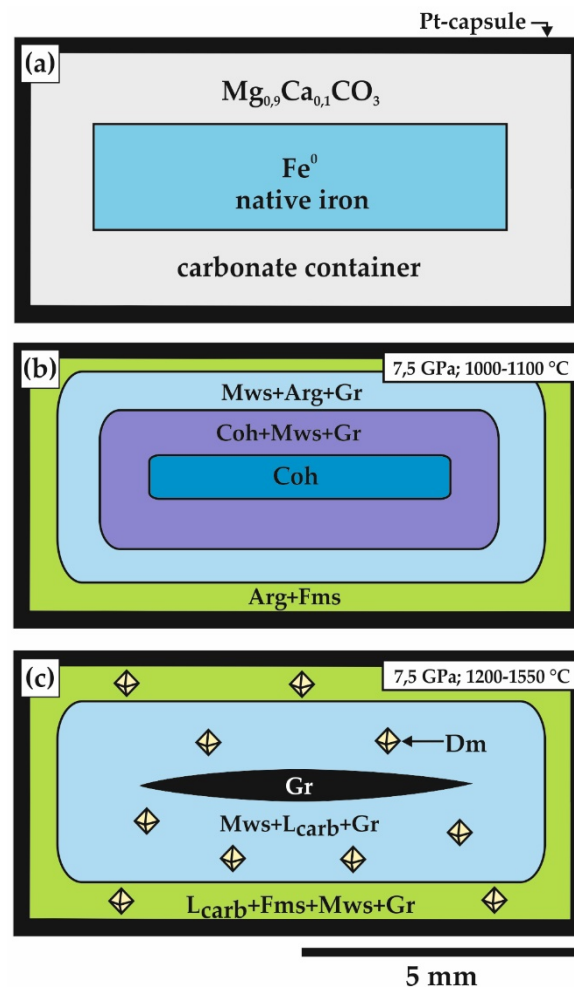


Figure 2. A scheme of an initial ampoule assembly (a) and schemes of ampoules after experiments on carbonate-metal interaction at 7.5 GPa and 1000–1100 °C (b) and 1200–1550 °C (c); Coh: cohenite, Mws: magnesiowustite, Arg: aragonite, Gr: graphite, Fms: ferromagnesite, Dm: diamond, L_{carb}: predominantly carbonate melt.

2.2. Methodical Approach for “Mixture-Type” Experiments

Experiments in the carbonate-iron-sulphur and carbide-oxide systems were carried out using an ampoule assembly design where all of the starting reagents were ground and homogenized. Natural magnesite and dolomite (<0.5 wt.% of impurities; Satka deposit, Urals, Russia), Fe⁰ and S (<0.01 wt.% of impurities) were used as starting reagents for the experiments in the carbonate-iron-sulphur system; pre-synthesized Fe₃C and synthetic Fe₂O₃ (<0.01 wt.% of impurities) were used as starting reagents for the experiments in the carbide-oxide system. Given the previous experience in the experimental studies involving iron-rich phases under mantle P and T, graphite was chosen as the optimal capsule material. During assembly, ground (up to 20–30 µm) and thoroughly mixed starting reagents were placed in graphite capsules; however, some carbide was not ground but placed in the ampoule as 300–500 µm crystalline fragments. To obtain information on diamond crystallization, seed cubo-octahedral diamond crystals (about 500 µm in size) were placed in ampoules.

2.3. Analytical Procedure

In all series of experiments, the magnesiowüstite composition was analysed by microprobe (Camebax-micro analyser, CAMECA, Gennevilliers, France). The analysis was performed using an accelerating voltage of 20 kV, a probe current of 20 nA, a counting time of 10 s in each analytical line and a probe electron beam diameter of 2–4 μm . Phase relations of magnesiowüstite with graphite, diamond, sulphides, silicates, carbide and quenched melts in produced samples were studied using scanning electron microscopy (SEM; Tescan MIRA3 LMU scanning electron microscope, TESCAN, Brno, Czech Republic). The measurements were performed at the Center for Collective Use of Multi-element and Isotopic Analysis of the Siberian Branch of the Russian Academy of Sciences (SB RAS).

In this study, Mössbauer spectroscopy was the main analytical method for the study of Fe^{3+} -bearing magnesiowüstite and wüstite. This method was used to determine the structure of magnesiowüstite and other iron-bearing phases, iron valence state in them and iron distribution in phases and non-equivalent positions. Mössbauer measurements were performed at the Kirensky Institute of Physics, SB RAS, Krasnoyarsk. Spectra were acquired at room temperature using an MS-1104Em spectrometer (Cordon, Rostov on Don, Russia) with a $\text{Co}^{57}(\text{Cr})$ source and a powder absorber thickness of 1–5 mg/cm^2 . Absorbers of this thickness are thin enough to avoid distortion of the area under a partial spectrum due to gamma ray self-absorption. The spectra were interpreted in two stages. At the first stage, quadrupole splittings $P(\text{QS})$ for doublets and probabilities of hyperfine fields $P(\text{H})$ for sextets were determined in experimental spectra. In this case, we fitted a chemical shift common to a group of doublets and a chemical shift and quadrupole splitting common to a group of sextets. The peaks and specific features of $P(\text{H})$ and $P(\text{QS})$ distributions demonstrate potential non-equivalent iron positions in the absorber. This set of information was used to generate a model spectrum that, at the second stage of interpretation, was fitted with an experimental spectrum by varying the entire set of hyperfine parameters. Upon this fitting, “false” sextets and doublets “vanish” and the parameters of true partial spectra are refined. The detected iron positions were assigned to a particular phase, based on similarity of the chemical shift and hyperfine field values and the appropriate parameters of known substances. The population of individual iron positions in the studied phase structure was estimated assuming that the Mössbauer effect probability was the same for all positions. The chemical shifts of positions are given with respect to that of metallic $\alpha\text{-Fe}$.

3. Results

3.1. Features of Fe^{3+} -Bearing Magnesiowüstite Formation in the Carbonate-Iron System

The results of experiments on the interaction between Mg,Ca-carbonate and iron, which simulate processes at the boundary between oxidized subducted material and reduced mantle rocks, were in detail described in Reference [63]. These experiments provided conditions for the formation of a redox front due to the $f\text{O}_2$ gradient in samples ($\Delta\log f\text{O}_2$ (FMQ) ≈ 4 units). Given the fact that magnesiowüstite was produced both ahead the front (at reducing conditions; in an assemblage with iron carbide, graphite or diamond; Table 1) and behind the front (at oxidizing conditions; in an assemblage with carbonates or predominantly carbonate melts, graphite or diamond), it seems topical to consider ferric iron distribution patterns in it. This section describes the characteristics of produced magnesiowüstite as a function of $f\text{O}_2$, based on the microprobe analysis and Mössbauer spectroscopy data. The composition of magnesiowüstite-bearing phase assemblages produced in the carbonate-iron system is shown in Table 1.

The sample structure in a relatively low-temperature experiment (1000 $^\circ\text{C}$, 7.5 GPa) is represented by alternating reaction zones (from a reduced center to an oxidized periphery): cohenite \rightarrow cohenite + magnesiowüstite + graphite \rightarrow magnesiowüstite + magnesioaragonite + graphite \rightarrow ferromagnesite + magnesioaragonite (Figures 2b and 3a,b). The produced magnesiowüstite is characterized by a variable composition: it is most iron-rich ($\text{Mg\#} = 0.12$) at the contact with carbide; at the contact with carbonates of the oxidized part of the sample, the MgO concentration in magnesiowüstite is 3-fold higher and the

magnesiowüstite composition changes to $Mg\# = 0.38$. Study of magnesiowüstite-bearing assemblages by Mössbauer spectroscopy revealed that under reducing conditions, in an assemblage with cohenite, all iron in magnesiowüstite was divalent; and in the most oxidized part of the sample, in an assemblage with carbonate, up to 30% of iron in magnesiowüstite was in the trivalent state ($Fe^{3+}/\Sigma Fe = 0.05\text{--}0.30$) (Table 3, Figure 4). Mössbauer spectra demonstrate concentration inhomogeneity of magnesiowüstite; they comprise areas with different contents of magnesium and cationic vacancies (Figures 4 and 5). In magnesiowüstite with a relatively low value of $Fe^{3+}/\Sigma Fe = 0.05$, Fe^{3+} is found to occupy tetrahedral positions in the structure. At very high Fe^{3+} concentrations, ferric iron occupies octahedral positions and also occurs in the nearest environment for one of the Fe^{2+} positions (with 1 cationic vacancy). At a higher temperature (1450 °C, 6.5 GPa), magnesiowüstite is formed mainly in the reduced zone of the sample (in an assemblage with cohenite and graphite) and only a small amount of (Fe,Mg)O is present in the oxidized part (in an assemblage with a predominantly carbonate melt and graphite) (Figure 3c,d). This melt is able to dissolve 15 (1200 °C) to 22 wt.% (1650 °C) of (Mg,Fe)O. Magnesiowüstite co-existing with carbide in the reduced zones of samples is significantly more iron-rich than that at the contact with the oxidized zone, in an assemblage with ferroaragonite. The magnesiowüstite composition within the reduced zone varies in an $Mg\#$ range of 0.27 to 0.30, with $Fe^{3+}/\Sigma Fe = 0.03$. Magnesiowüstite in the oxidized zone is more magnesian than that in the reduced one, with $\Delta Mg\#$ being 0.03–0.09. The Fe^{3+} contents in it are extremely high, with $Fe^{3+}/\Sigma Fe = 0.34$.

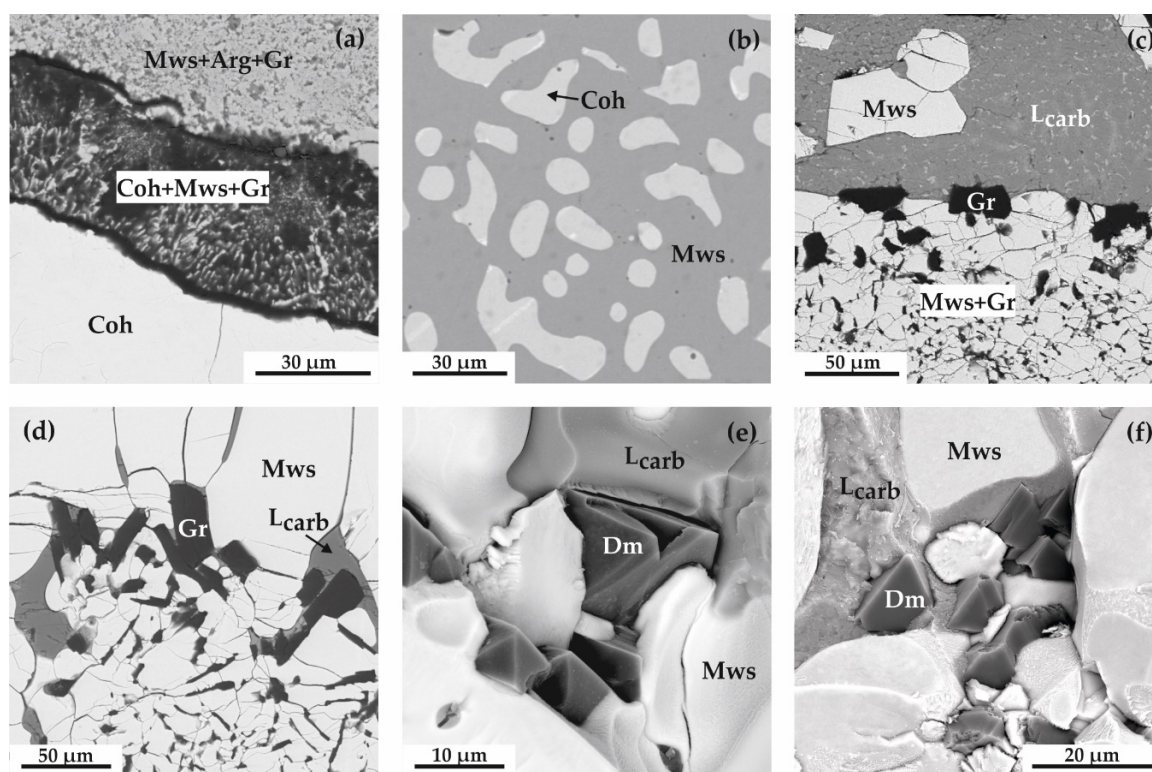


Figure 3. Scanning electron microscopy (SEM) photographs of sample fragments, which were produced in the carbonate-iron system: (a) graphite, cohenite and magnesiowüstite (reaction zone) at the contact between coarse-grained cohenite and a fine-grained magnesiowüstite + aragonite + graphite aggregate (1000 °C, 7.5 GPa); (b) assemblage of magnesiowüstite and cohenite (reduced zone) (1450 °C, 6.5 GPa); (c) crystals of magnesiowüstite and graphite in a quenched carbonate melt (1450 °C, 6.5 GPa); (d) crystals of magnesiowüstite and graphite, with quenching carbonate in interstices (1450 °C, 6.5 GPa); (e, f) diamond crystals and quenching carbonate in coarse-grained magnesiowüstite interstices (1550 °C, 7.5 GPa). Coh: cohenite, Mws: magnesiowüstite, Arg: aragonite, Gr: graphite, Dm: diamond, L_{carb}: predominantly carbonate melt.

In a temperature range of 1400–1550 °C (7.5 GPa, Figure 2c, Figure 3e,f), the magnesiowüstite composition in the reduced and oxidized zones is almost constant ($\Delta\text{Mg\#} < 0.01$). Magnesiowüstite from the reduced part of samples is characterized by Mg\# 0.37 (1400 °C) and 0.42 (1550 °C), with 3–13% ($\pm 2\%$, after probability distributions of QS fitting) of iron in the magnesiowüstite being in the trivalent state ($\text{Fe}^{3+}/\sum\text{Fe} = 0.03\text{--}0.13$). Magnesiowüstite in the oxidized zone is more magnesian, with $\Delta\text{Mg\#}$ of the reduced and oxidized zones being 0.01 to 0.02. It contains from 3–11 (1400 °C) to 13% (1550 °C) of Fe^{3+} ($\pm 2\%$, after probability distributions of QS fitting). At these parameters, ferric iron occupies predominantly tetrahedral positions in the structure of magnesiowüstite. In general, magnesiowüstite formed in the carbonate-iron system contains up to 4 groups of Fe^{2+} cation positions with different symmetry of the local environment. As demonstrated in Reference [72], these positions are associated with a different number of cationic vacancies among the nearest surrounding. Detailed cationic vacancy distribution in the magnesiowüstite structure is given in Table 3.

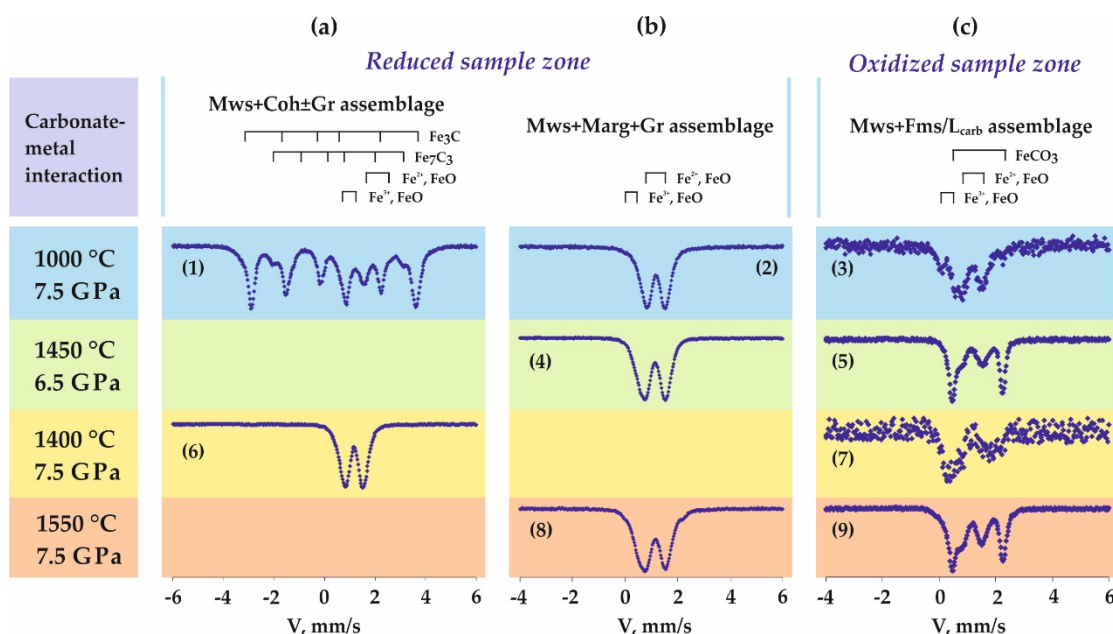


Figure 4. Mössbauer spectra of samples from reduced (1,2,4,6,8) and oxidized (3,5,7,9) zones, which were produced in experiments in the carbonate-iron system. (a,b)—assemblages of reduced sample zones, (c)—assemblages of oxidized sample zone.

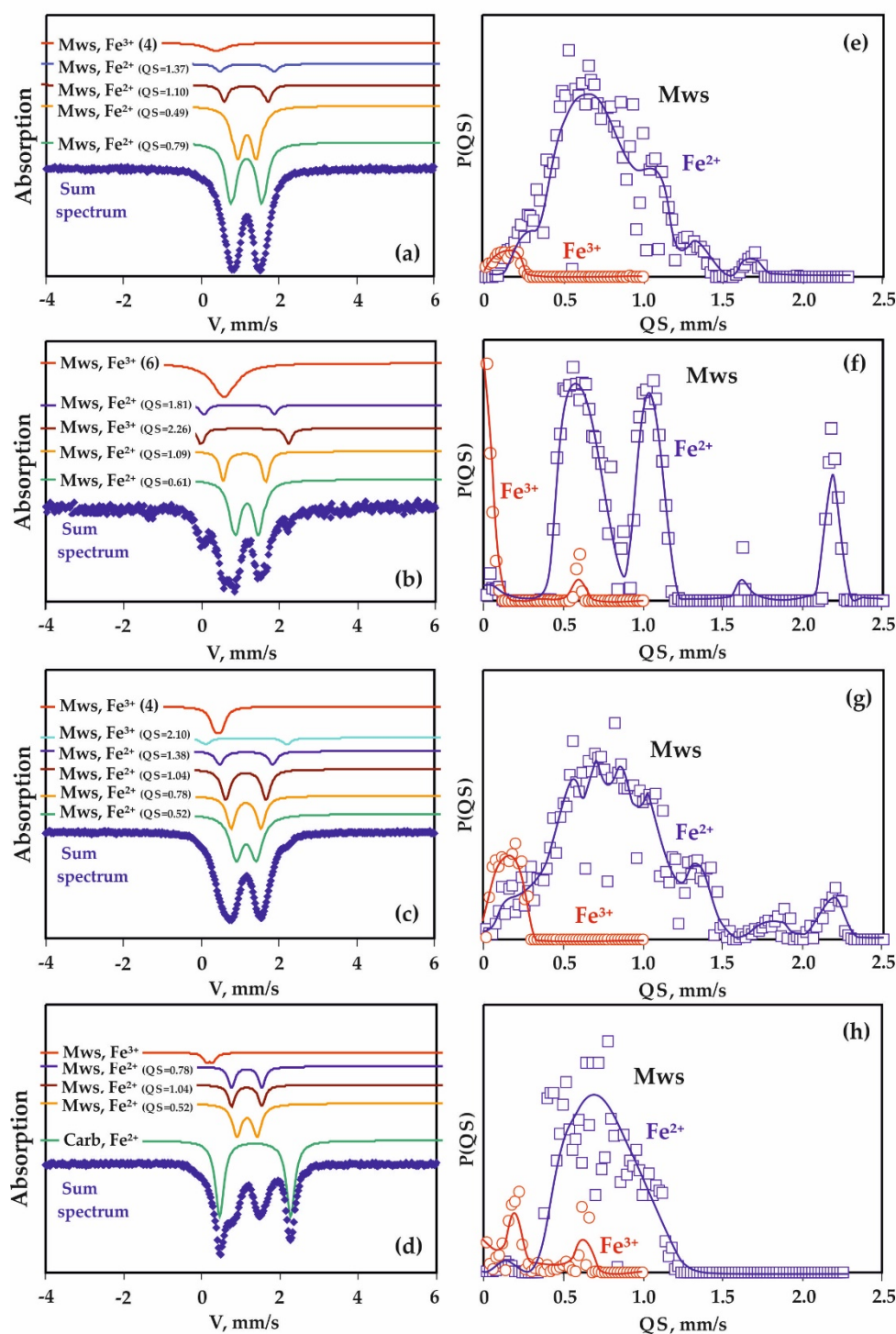


Figure 5. Mössbauer spectra of samples produced in the carbonate-iron system (exp. 1541 (a,b,e,f) and 1515 (c,d,g,h)) as well as components of these spectra (a–d) and the probability distribution of quadrupole splittings P(QS) in experimental spectra of magnesiowüstite (e–h).

Table 3. Results of the Mössbauer spectroscopy of magnesiowüstite and wüstite formed in the carbonate-metal system.

Run N	Sample Zone	Phase	Fe Positions	A, % (± 2)	IS, mm/s ± 0.02	QS, mm/s ± 0.04	W, mm/s ± 0.04
1541	Reduced	Ws	Fe ²⁺ in FeO	26	1.02	0.35	0.37
			Fe ²⁺ in Fe _{1-y} Mg _y O	40	1.00	0.68	0.29
		Mws	Fe ²⁺ in (Fe _{1-y} Mg _y) _x O	14	0.95	1.02	0.22
			Fe ²⁺ in (Fe _{1-y} Mg _y) _x O, high y	20	0.88	1.19	0.42
	Oxidized	Mws	Fe ²⁺ in (Fe _{1-y} Mg _y)O (N _{CV} = 0)	37	1.02	0.49	0.32
			Fe ²⁺ in (Fe _{1-y} Mg _y) _x O (N _{CV} = 1)	44	1.02	0.79	0.32
			Fe ²⁺ in (Fe _{1-y} Mg _y) _x O (N _{CV} = 2)	9	1.00	1.10	0.22
			Fe ²⁺ in (Fe _{1-y} Mg _y) _x O (N _{CV} = 3)	5	1.02	1.37	0.27
			Fe ³⁺ (IV) in (Fe _{1-y} Mg _y) _x O	5	0.24	0.23	0.49
	Oxidized	Mws	Fe ²⁺ in (Fe _{1-y} Mg _y)O (N _{CV} = 0)	42	1.02	0.61	0.33
			Fe ²⁺ in (Fe _{1-y} Mg _y) _x O (N _{CV} = 1)	15	0.96	1.09	0.21
			Fe ²⁺ in (Fe _{1-y} Mg _y) _x O (N _{CV} = 2)	5	0.81	1.81	0.20
			Fe ²⁺ in (Fe _{1-y} Mg _y) _x O (N _{CV} = 1 + Fe ³⁺)	8	0.97	2.26	0.21
			Fe ³⁺ (VI) in (Fe _{1-y} Mg _y) _x O	30	0.43	0	0.74
1250	Reduced	Mws	Fe ²⁺ in (Fe _{1-y} Mg _y)O (N _{CV} =0)	28	1.00	0.45	0.24
			Fe ²⁺ in (Fe _{1-y} Mg _y) _x O (N _{CV} =1)	31	1.01	0.69	0.23
			Fe ²⁺ in (Fe _{1-y} Mg _y) _x O (N _{CV} =2)	21	1.00	0.93	0.22
			Fe ²⁺ in (Fe _{1-y} Mg _y) _x O (N _{CV} =3)	17	0.99	1.21	0.28
			Fe ³⁺ (VI) in (Fe _{1-y} Mg _y) _x O	3	0.52	0.68	0.22
	Oxidized	Mws	Fe ²⁺ in (Fe _{1-y} Mg _y) _x O	66	1.09	1.22	0.56
			Fe ³⁺ (IV) in (Fe _{1-y} Mg _y) _x O	34	0.13	-	0.39
	Reduced	Mws	Fe ²⁺ in (Fe _{1-y} Mg _y)O (N _{CV} = 0)	34	0.98	0.51	0.32
			Fe ²⁺ in (Fe _{1-y} Mg _y) _x O (N _{CV} = 1)	26	0.98	0.77	0.24
			Fe ²⁺ in (Fe _{1-y} Mg _y) _x O (N _{CV} = 2)	22	0.97	1.05	0.23
			Fe ²⁺ in (Fe _{1-y} Mg _y) _x O (N _{CV} = 3)	9	0.96	1.40	0.22
			Fe ³⁺ (IV) in (Fe _{1-y} Mg _y) _x O	9	0.23	0.23	0.24
1525	Oxidized	Mws	Fe ²⁺ in (Fe _{1-y} Mg _y)O (N _{CV} = 0)	56	1.19	1.79	0.22
			Fe ²⁺ in (Fe _{1-y} Mg _y) _x O (N _{CV} = 1)	19	0.99	0.54	0.27
			Fe ²⁺ in (Fe _{1-y} Mg _y) _x O (N _{CV} = 2)	10	0.98	0.82	0.20
			Fe ²⁺ in (Fe _{1-y} Mg _y) _x O (N _{CV} = 3)	12	0.97	1.11	0.23
			Fe ³⁺ (IV) in (Fe _{1-y} Mg _y) _x O	3	0.15	0.11	0.08
	Reduced	Mws	Fe ²⁺ in (Fe _{1-y} Mg _y)O (N _{CV} = 0)	38	1.01	0.52	0.39
			Fe ²⁺ in (Fe _{1-y} Mg _y) _x O (N _{CV} = 1)	20	1.00	0.78	0.27
			Fe ²⁺ in (Fe _{1-y} Mg _y) _x O (N _{CV} = 2)	19	0.99	1.04	0.28
			Fe ²⁺ in (Fe _{1-y} Mg _y) _x O (N _{CV} = 3)	8	1.00	1.38	0.27
			Fe ²⁺ in (Fe _{1-y} Mg _y) _x O (N _{CV} = 1 + Fe ³⁺)	4	1.01	2.10	0.27
			Fe ³⁺ (IV) in (Fe _{1-y} Mg _y) _x O	11	0.27	0.17	0.27
1515	Oxidized	Mws	Fe ²⁺ in (Fe _{1-y} Mg _y)O (N _{CV} =0)	47	1.00	0.52	0.28
			Fe ²⁺ in (Fe _{1-y} Mg _y) _x O (N _{CV} =1)	22	1.00	0.78	0.21
			Fe ²⁺ in (Fe _{1-y} Mg _y) _x O (N _{CV} =2)	18	1.00	1.04	0.23
			Fe ³⁺ (IV-VI) in (Fe _{1-y} Mg _y) _x O	13	0.27	0.29	0.23

Mws: magnesiowüstite, Ws: wüstite; IS: Isomer shift (mm/s) with reference to α -Fe; QS: Quadrupole splitting (mm/s); W: Width of the absorption line (mm/s); A: (Area(Fe³⁺)/(Area(Fe²⁺) + Area(Fe³⁺)) \times 100 or (Area(Fe²⁺)/(Area(Fe²⁺) + Area(Fe³⁺)) \times 100; Number in parenthesis: (IV) or (VI) denotes coordination number; N_{CV}: number of cation vacancies in the closest surrounding of Fe²⁺.

3.2. Features of Fe³⁺-Bearing Magnesiowüstite Formation in the Carbonate-Oxide-Metal System

The results of experiments in carbonate-oxide-metal system simulating the interaction between Fe⁰-bearing rocks and carbonated rocks, which is associated with the generation of Fe³⁺-enriched carbonate-silicate melts, are in detail described in Reference [64]. The produced samples were characterized by a zonal structure due to the fO_2 gradient in the reaction volume (Figure 6).

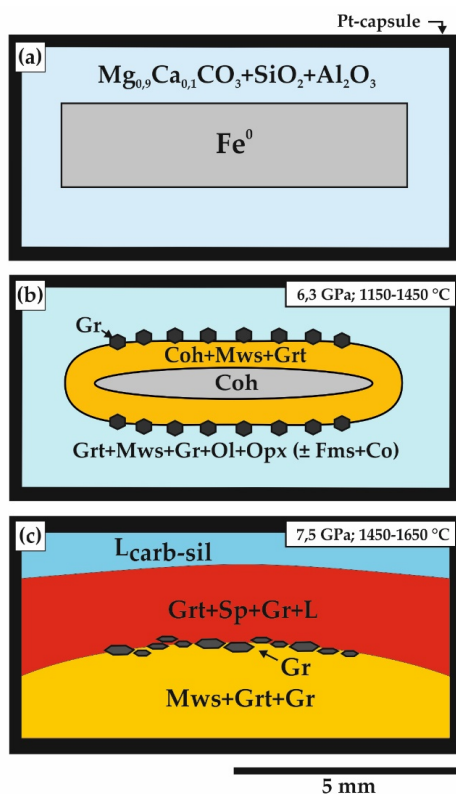


Figure 6. A scheme of an initial ampoule assembly (a) and schemes of ampoules after experiments on carbonate-oxide-metal interaction at 6.3 GPa and 1150–1450 °C (b) and 7.5 GPa and 1450–1650 °C (c); Coh: cohenite, Mws: magnesiowüstite, Grt: garnet, Ol: olivine, Gr: graphite, Fms: ferromagnesite, Opx: orthopyroxene, Co: coesite, Sp: spinel, L_{carb-sil}: carbonate-silicate melt.

In a temperature range of 1050–1450 °C (6.3 GPa), magnesiowüstite was produced in an assemblage with cohenite, almandine and graphite in the reduced zone and in an assemblage with pyrope-almandine, olivine, carbonate and graphite in the oxidized zone (Figures 6b and 7a–c). The composition of magnesiowüstite formed in the reduced zone varies from $\text{Fe}_{0.83}\text{Mg}_{0.17}\text{O}$ (1150 °C) to $\text{Fe}_{0.76}\text{Mg}_{0.24}\text{O}$ (1450 °C), while its composition in the oxidized part of ampoules almost does not depend on temperature and corresponds to about $\text{Fe}_{0.81}\text{Mg}_{0.19}\text{O}$. The Mössbauer parameters of produced magnesiowüstite (Table 4; Figures 8 and 9) are in good agreement with the literature data [73,74]. Magnesiowüstite is the main iron-bearing phase in a temperature range of 1050–1450 °C; it contains up to 84% of the total iron in the system. In both the oxidized and reduced parts of samples, ~5–7% of iron in magnesiowüstite occurs in the trivalent state and occupies tetrahedral positions in the structure. The distribution of quadrupole splittings P(QS) occupies a rather wide range (Figure 9c,f), indicating significant inhomogeneities in the distribution of cationic vacancies. In all studied samples, 1 to 3 different Fe^{2+} positions were found (Table 4), indicating a variable number of vacancies, their high concentration and their uneven distribution in the structure of magnesiowüstite.

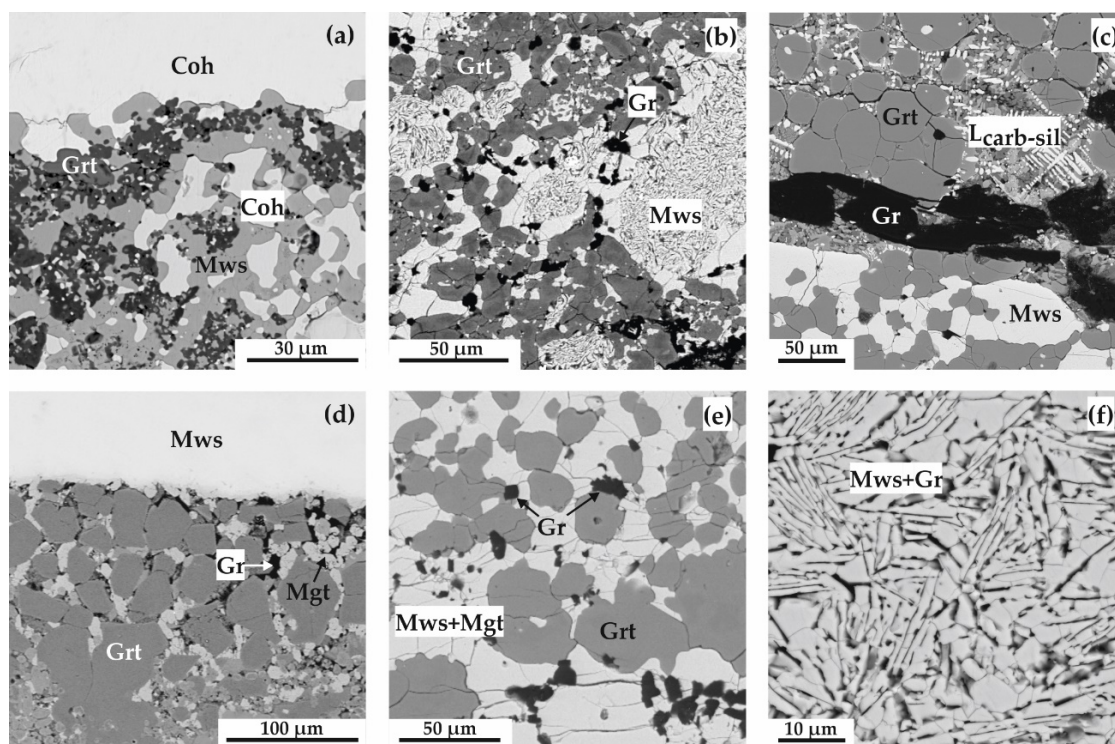


Figure 7. SEM photographs of sample fragments produced in carbonate-oxide-metal (a–c) and carbonate-oxide (d–f) systems: (a) reduced zone (cohenite + magnesiowüstite + garnet) (1150 °C); (b) oxidized zone (magnesiowüstite + garnet + graphite) (1450 °C); (c) (bottom) polycrystalline aggregate of magnesiowüstite, garnet and graphite; (top) – garnet and graphite in a quenching aggregate (1550 °C); (d) reaction zone consisting of almandine, graphite and magnetite at the contact with magnesiowüstite (1150 °C); (e) polycrystalline aggregate of magnesiowüstite, magnetite, graphite and garnet (1250 °C); (f) polycrystalline aggregate of magnesiowüstite and graphite (1350 °C); Coh: cohenite, Grt: garnet, Mws: magnesiowüstite, Mgt: magnetite, Gr: graphite, $L_{\text{carb-sil}}$: carbonate-silicate melt.

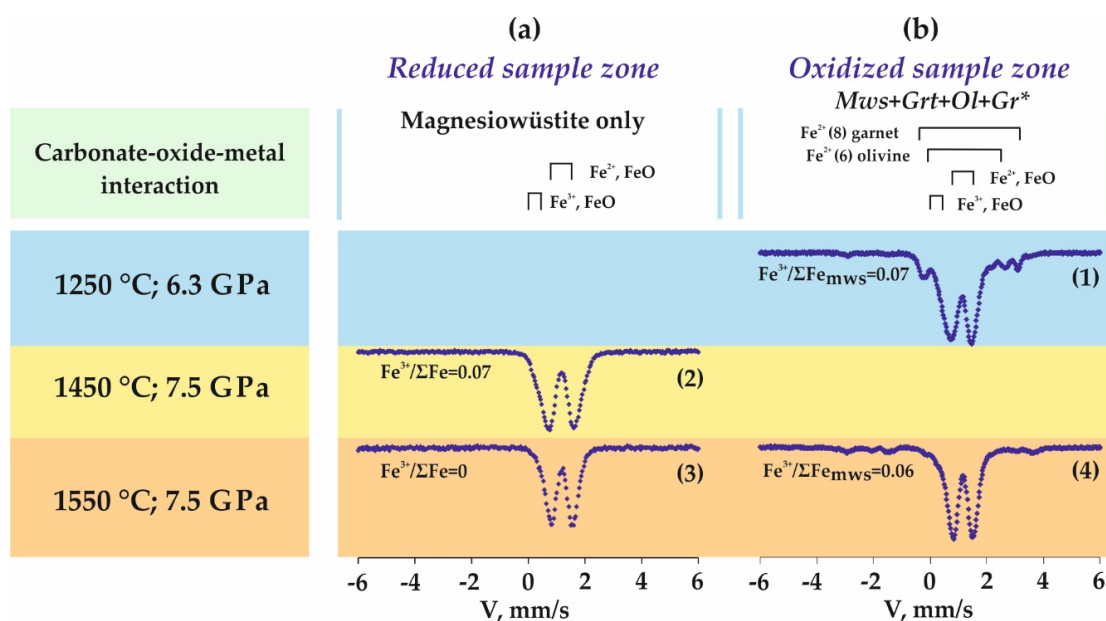


Figure 8. Mössbauer spectra of samples from reduced (2,4) and oxidized (1,3) zones, which were produced in experiments in the carbonate-oxide-metal system. (a) assemblages of reduced sample zone, (b) assemblages of oxidized sample zone.

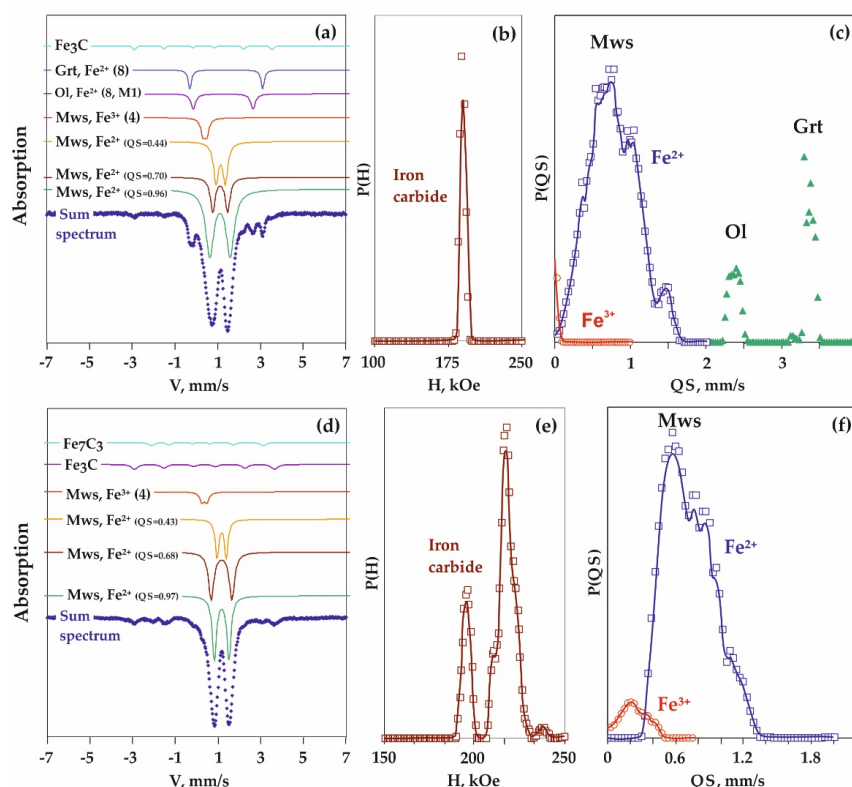


Figure 9. Mössbauer spectra of samples produced in the carbonate-iron system (N. 1287 (a–c) and 1249 (d–f)) as well as components of these spectra (a,d), the probability distribution of hyperfine magnetic fields (H) on iron nuclei (b,e) and the probability distribution of quadrupole splittings P(QS) in experimental spectra of magnesiowüstite and silicates (c,f).

Table 4. Results of the Mössbauer spectroscopy of magnesiowüstite formed in the carbonate-oxide-metal and carbonate-oxide systems ($P = 6.3$ GPa).

Run N	Sample Zone	Phase	Fe Positions	A, % (± 2)	IS, mm/s ±0.02	QS, mm/s ±0.04	W, mm/s ±0.04
Carbonate-oxide-metal system							
1287	Reduced	Mws	Fe ²⁺ in (Fe _{1-y} Mg _y)O (N _{CV} = 0)	21	0.99	0.44	0.28
			Fe ²⁺ in (Fe _{1-y} Mg _y) _x O (N _{CV} = 1)	16	0.97	0.70	0.27
			Fe ²⁺ in (Fe _{1-y} Mg _y) _x O (N _{CV} = 2)	55	0.96	0.96	0.46
			Fe ³⁺ (IV) in (Fe _{1-y} Mg _y) _x O	7	0.25	0.18	0.25
	Oxidized	Mws	Fe ²⁺ in (Fe _{1-y} Mg _y) _x O	93	0.97	0.75	0.49
			Fe ³⁺ (IV) in (Fe _{1-y} Mg _y) _x O	7	0.26	0.17	0.19
1250-2	Reduced	Mws	Fe ²⁺ in (Fe _{1-y} Mg _y)O (N _{CV} = 0)	20	1.02	0.49	0.32
			Fe ²⁺ in (Fe _{1-y} Mg _y) _x O (N _{CV} = 1)	39	1.02	0.79	0.32
			Fe ²⁺ in (Fe _{1-y} Mg _y) _x O (N _{CV} = 2)	36	1.00	1.10	0.22
			Fe ³⁺ (IV) in (Fe _{1-y} Mg _y) _x O	5	1.02	1.37	0.27
	Carbonate-oxide system						
1289	Reduced	Mws	Fe ²⁺ in (Fe _{1-y} Mg _y) _x O	95	1.06	0.73	0.46
			Fe ³⁺ (IV) in (Fe _{1-y} Mg _y) _x O	5	0.16	0.53	0.21
1287-2	Reduced	Mws	Fe ²⁺ in (Fe _{1-y} Mg _y) _x O	93	1.03	0.94	0.50
			Fe ³⁺ (IV) in (Fe _{1-y} Mg _y) _x O	7	0.16	0.19	0.23
1283	Reduced	Mws	Fe ²⁺ in (Fe _{1-y} Mg _y) _x O	88	1.06	0.71	0.46
			Fe ³⁺ (IV) in (Fe _{1-y} Mg _y) _x O	12	0.18	0.52	0.33

Mws: magnesiowüstite; IS: Isomer shift (mm/s) with reference to $\alpha\text{-Fe}$; QS: Quadrupole splitting (mm/s); W: Width of the absorption line (mm/s); A: $(\text{Area}(\text{Fe}^{3+})/(\text{Area}(\text{Fe}^{2+}) + \text{Area}(\text{Fe}^{3+})) \times 100$ or $(\text{Area}(\text{Fe}^{2+})/(\text{Area}(\text{Fe}^{2+}) + \text{Area}(\text{Fe}^{3+})) \times 100$; Number in parenthesis: (IV) or (VI) denotes coordination number; N_{CV} : number of cation vacancies in the closest surrounding of Fe^{2+} .

At higher temperatures (in the presence of a carbonate-silicate melt), as a result of lack of metallic iron or iron carbide, there is no separation into the reduced and oxidized parts of samples after experiments (Figure 6c). Under these conditions, magnesiowüstite is present only in an assemblage with magnetite, garnet and metastable graphite. The magnesiowüstite composition is characterized by a decrease in the iron content as temperature increases, from Fe# 0.88 (1450 °C) to Fe# 0.76 (1650 °C). According to Mössbauer spectroscopy, under these conditions, magnesiowüstite lacks Fe³⁺ and ferric iron-concentrating phases include magnetite, ferrosipinel and garnet.

3.3. Features of Fe³⁺-Bearing Magnesiowüstite Formation in the Carbonate-Oxide System

The results of carbonate-oxide interaction experiments simulating the interaction between magnesiowüstite and oxidizing metasomatic agents (CO₂ fluid and carbonate-silicate melt) are in detail described in Reference [65]. A zonal structure of produced samples is shown in Figure 10.

Magnesiowüstite is formed in the system in a temperature range of 1150–1350 °C. At relatively low temperatures (1150–1250 °C), magnesiowüstite is produced in the central (reduced) part of samples (Figures 7d–e and 10b) and is surrounded by a reaction zone consisting of almandine, magnetite and graphite (Figure 7d–f). The reaction zone width increases with the temperature; in this case, the amount of coarse-grained magnesiowüstite in the central part of ampoules decreases. At 1350 °C, magnetite is found not only in the reaction zone but also in the central part of an ampoule, in an assemblage with magnesiowüstite. In this case, the carbonate-oxide ampoule is replaced by an assemblage of pyrope-almandine + magnesiowüstite + magnetite + ferrosilite + ferromagnesite + graphite, where magnesiowüstite is found in intergrowths with graphite (Figure 7c). In the composition of produced magnesiowüstite, Mg# consistently increases with the temperature, from 0.01 (1150 °C) to 0.13 (1350 °C). Samples of coarse-grained magnesiowüstite from the reduced zones were analysed by Mössbauer spectroscopy (Table 4; Figure 11). The obtained spectra of wüstite are similar to those presented in References [73,74] for Fe_xO, with $x \sim 0.96$. Four different Fe²⁺ positions detected in each sample indicate an uneven distribution and a variable number of cationic vacancies in the structure. The Fe³⁺ content in magnesiowüstite is found to be directly dependent on the temperature and vary from 5 (1150 °C) to 12 at.% (1350 °C) (Table 4). In this case, Fe³⁺ is tetrahedrally coordinated.

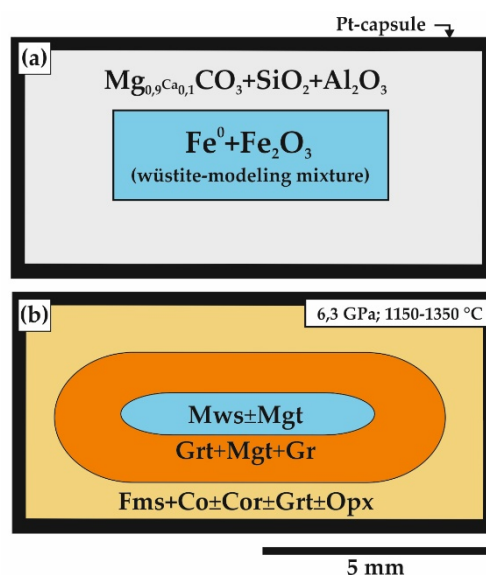


Figure 10. A scheme of an initial ampoule assembly (a) and scheme of ampoule after experiments on carbonate-oxide interaction (b); Mws: magnesiowüstite, Mgt: magnetite, Grt: garnet, Opx: orthopyroxene, Gr: graphite, Fms: ferromagnesite, Co: coesite, Cor: corundum.

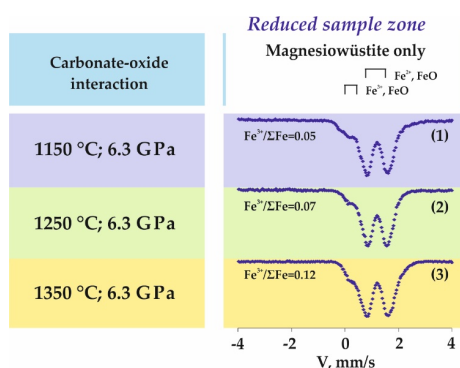


Figure 11. Mössbauer spectra of magnesiowüstite from reduced zones of samples produced in experiments in the carbonate-oxide system.

3.4. Features of Fe^{3+} -Bearing Wüstite Formation in the Carbide-Oxide System

The interaction of cohenite and hematite in a temperature range of 900–1600 °C ($P = 6.3$ GPa) is found to result in the formation of Fe^{3+} -bearing magnesiowüstite and graphite assemblage (Table 5).

At $T < 1300$ °C, single cohenite crystals surrounded by graphite reaction rims remain in samples (Figure 12a,b). At $T \geq 1400$ °C, a small amount (<5 wt.%) of Fe–C melt is formed, with large graphite crystals (up to 100 μm) being associated with quenching aggregates of the melt (Figure 12c). The size of produced Fe^{3+} -bearing wüstite crystals increases as the temperature of experiments is raised, from 10–100 μm (900 °C) to 0.5 mm (1600 °C). The wüstite composition corresponds to $\sim\text{Fe}_{0.95-0.97}\text{O}$ and wüstite is characterized by numerous cationic vacancies and Fe^{3+} concentrations of ~ 2 –4 at.%, which are temperature-independent. Ferric iron in wüstite produced by the carbide–hematite interaction is VI coordinated (Table 5, Figure 13). Four different positions of Fe^{2+} in the magnesiowüstite structure, which are found at all temperatures, indicate a variable number of vacancies, their high concentration and their uneven distribution.

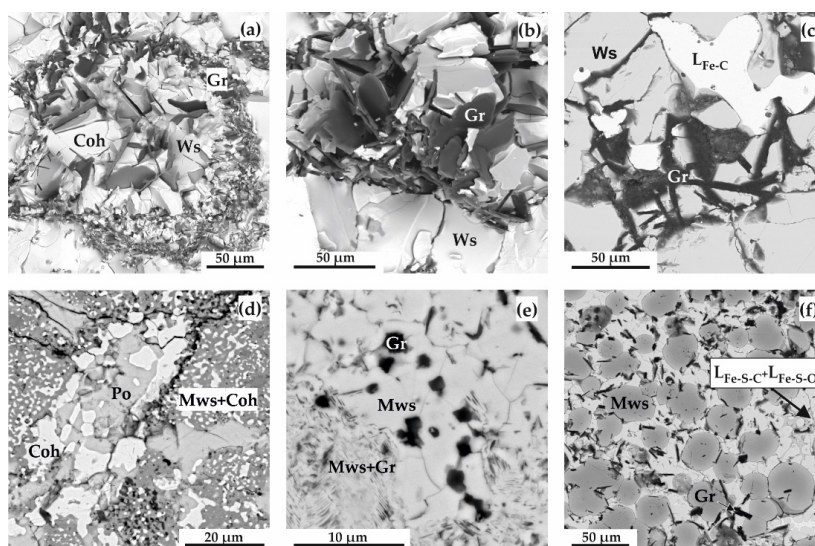


Figure 12. SEM photographs of sample fragments, which were produced in cohenite-hematite (a–c) and carbonate-iron-sulphur (d–f) systems: (a): cleavage surface; graphite and wüstite reaction zone around cohenite (1200 °C); (b): cleavage surface; graphite crystals in a wüstite aggregate (1500 °C); (c): graphite crystals and quenched iron-carbon melt pools in a wüstite aggregate (1500 °C); (d): polycrystalline aggregate of cohenite, pyrrhotite and magnesiowüstite (900 °C); (e): polycrystalline aggregate of magnesiowüstite and graphite (1100 °C); (f) rounded magnesiowüstite crystals and graphite plates in quenching Fe–S–O and Fe–S–C melts (1600 °C); Ws: wüstite, Mws: magnesiowüstite, Po: pyrrhotite, Coh: cohenite, Gr: graphite, $L_{\text{Fe-C}}$: iron-carbon melt, $L_{\text{Fe-S-C}}$: Fe–S–C melt; $L_{\text{Fe-S-O}}$: Fe–S–O melt.

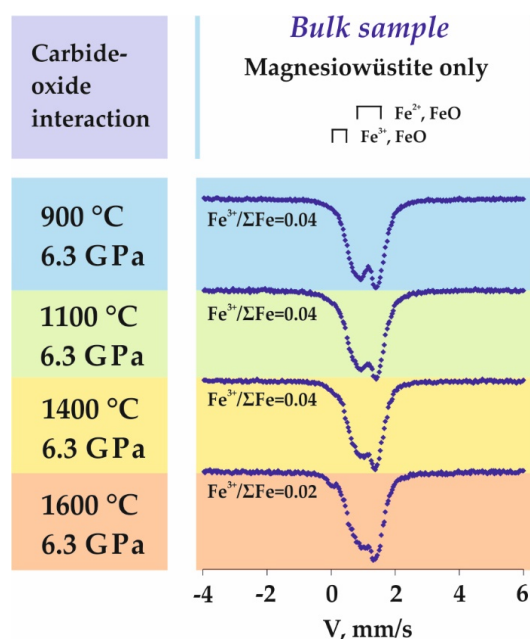


Figure 13. Mössbauer spectra of wüstite produced in the carbide-oxide system.

Table 5. Results of the Mössbauer spectroscopy of wüstite and magnesiowüstite formed in the carbide-oxide and carbonate-metal-sulphur systems ($P = 6.3$ GPa).

Run N	Phase	Fe Positions	A, % ±2	IS, mm/s ±0.02	QS, mm/s ±0.04	W, mm/s ±0.04
Carbide-oxide system						
1623-A4	Ws	Fe ²⁺ in FeO (N _{CV} = 0)	27	0.96	0.38	0.32
		Fe ²⁺ in Fe _x O (N _{CV} = 1)	11	1.14	0.38	0.22
		Fe ²⁺ in Fe _x O (N _{CV} = 2)	32	0.89	0.61	0.41
		Fe ²⁺ in Fe _x O (N _{CV} = 3)	26	0.92	1.04	0.41
		Fe ³⁺ (VI) in Fe _x O	4	0.36	1.02	0.21
1620-A4	Ws	Fe ²⁺ in FeO (N _{CV} = 0)	30	0.95	0.35	0.32
		Fe ²⁺ in Fe _x O (N _{CV} = 1)	15	1.12	0.38	0.24
		Fe ²⁺ in Fe _x O (N _{CV} = 2)	24	0.91	0.64	0.33
		Fe ²⁺ in Fe _x O (N _{CV} = 3)	27	0.93	1.06	0.37
		Fe ³⁺ (VI) in Fe _x O	4	0.32	0.75	0.31
1618-A4	Ws	Fe ²⁺ in FeO (N _{CV} = 0)	26	0.96	0.31	0.36
		Fe ²⁺ in Fe _x O (N _{CV} = 1)	7	1.09	0.31	0.22
		Fe ²⁺ in Fe _x O (N _{CV} = 2)	23	0.98	0.62	0.38
		Fe ²⁺ in Fe _x O (N _{CV} = 3)	40	0.93	0.96	0.48
		Fe ³⁺ (VI) in Fe _x O	4	0.17	0.58	0.53
1602-A4	Ws	Fe ²⁺ in FeO (N _{CV} = 0)	20	0.97	0.34	0.36
		Fe ²⁺ in Fe _x O (N _{CV} = 1)	8	1.09	0.40	0.24
		Fe ²⁺ in Fe _x O (N _{CV} = 2)	38	0.94	0.60	0.43
		Fe ²⁺ in Fe _x O (N _{CV} = 3)	32	0.94	1.02	0.43
		Fe ³⁺ (VI) in Fe _x O	2	0.40	0.80	0.33
Carbonate-metal-sulphur system						
MCS-23	Mws	Fe ²⁺ in (Fe ₁ – _y Mg _y)O (N _{CV} = 0)	27	1.07	0.52	0.31
		Fe ²⁺ in (Fe ₁ – _y Mg _y) _x O (N _{CV} = 1)	49	1.06	0.82	0.35
		Fe ²⁺ in (Fe ₁ – _y Mg _y) _x O (N _{CV} = 2)	16	1.08	1.22	0.30
		Fe ³⁺ (IV) in (Fe ₁ – _y Mg _y) _x O	8	0.11	0.38	0.34

Table 5. Cont.

Run N	Phase	Fe Positions	A, % ±2	IS, mm/s ±0.02	QS, mm/s ±0.04	W, mm/s ±0.04
Carbonate-metal-sulphur system						
MCS-20	Mws	Fe ²⁺ in (Fe _{1-y} Mg _y)O (N _{CV} = 0)	19	1.07	0.61	0.29
		Fe ²⁺ in (Fe _{1-y} Mg _y) _x O (N _{CV} = 1)	47	1.07	0.99	0.41
		Fe ²⁺ in (Fe _{1-y} Mg _y) _x O (N _{CV} = 2)	20	1.06	1.48	0.39
		Fe ²⁺ in (Fe _{1-y} Mg _y) _x O (N _{CV} = 3)	8	1.02	2.12	0.27
		Fe ³⁺ (IV and VI) in (Fe _{1-y} Mg _y) _x O	5	0.27 0.25	0.39 0.78	0.30 0.20
MCS-18	Mws	Fe ²⁺ in (Fe _{1-y} Mg _y)O (N _{CV} = 0)	35	1.04	0.55	0.33
		Fe ²⁺ in (Fe _{1-y} Mg _y) _x O (N _{CV} = 1)	45	1.04	0.83	0.33
		Fe ²⁺ in (Fe _{1-y} Mg _y) _x O (N _{CV} = 2)	5	1.04	1.27	0.23
		Fe ²⁺ in (Fe _{1-y} Mg _y) _x O (N _{CV} = 3)	8	1.00	1.37	0.40
		Fe ³⁺ (IV) in (Fe _{1-y} Mg _y) _x O	7	0.19	0.60	0.23
MCS-02	Mws	Fe ²⁺ in (Fe _{1-y} Mg _y)O (N _{CV} = 0)	52	1.01	0.59	0.34
		Fe ²⁺ in (Fe _{1-y} Mg _y) _x O (N _{CV} = 1)	18	1.01	0.90	0.24
		Fe ²⁺ in (Fe _{1-y} Mg _y) _x O (N _{CV} = 2)	16	1.00	1.27	0.30
		Fe ³⁺ (VI) in (Fe _{1-y} Mg _y) _x O	13	0.38	0.91	0.35

Mws: magnesiowüstite, Ws: wüstite; IS: Isomer shift (mm/s) with reference to α -Fe; QS: Quadrupole splitting (mm/s); W: Width of the absorption line (mm/s); A: $(\text{Area}(\text{Fe}^{3+})/(\text{Area}(\text{Fe}^{2+}) + \text{Area}(\text{Fe}^{3+}))) \times 100$ or $(\text{Area}(\text{Fe}^{2+})/(\text{Area}(\text{Fe}^{2+}) + \text{Area}(\text{Fe}^{3+}))) \times 100$; Number in parenthesis: (IV) or (VI) denotes coordination number; N_{CV}: number of cation vacancies in the closest surrounding of Fe²⁺.

3.5. Features of Fe³⁺-Bearing Magnesiowüstite Formation in the Carbonate-Iron-Sulfur System

At relatively low temperatures (900 and 1000 °C), the carbonate-iron-sulphur interaction leads to the formation of polycrystalline magnesiowüstite + cohenite + graphite aggregates (Figure 12d) as well as pyrrhotite and Fe,Mg,Ca-carbonate. The magnesiowüstite composition in these conditions corresponds to Fe_{0.69}Mg_{0.31}O (900 °C) and Fe_{0.75}Mg_{0.25}O (1000 °C); magnesiowüstite contains ~8 at.% of ferric iron (Table 5). In a range of 1100–1200 °C, an assemblage of magnesiowüstite, pyrrhotite and graphite is formed. Graphite is present in samples as intergrowths with magnesiowüstite or as inclusions in magnesiowüstite (Figure 12e). At T ≥ 1300 °C a solid-phase assemblage of magnesiowüstite + graphite is formed and two melts, Fe–S–C and Fe–S–O, are generated. Magnesiowüstite produced in this temperature range occurs as rounded crystals with inclusions of graphite plates (Figure 12e). The magnesiowüstite composition in a range of 1100–1400 °C corresponds to Fe_{0.61–0.63}Mg_{0.29–0.33}Ca_{0.06–0.08}O. The results of sample analysis using Mössbauer spectroscopy are shown in Figures 14 and 15. In this range, Fe³⁺/ΣFe values increase from 0.05 to 0.07, depending on the temperature. At higher temperatures, magnesiowüstite crystals are zonal and characterized by a Mg-rich central part (~Fe_{0.51}Mg_{0.44}Ca_{0.06}O, Fe³⁺/ΣFe ~0.08) and a Fe-rich periphery (~Fe_{0.79–0.83}Mg_{0.17–0.21}O, Fe³⁺/ΣFe ~0.13) (Figure 12f).

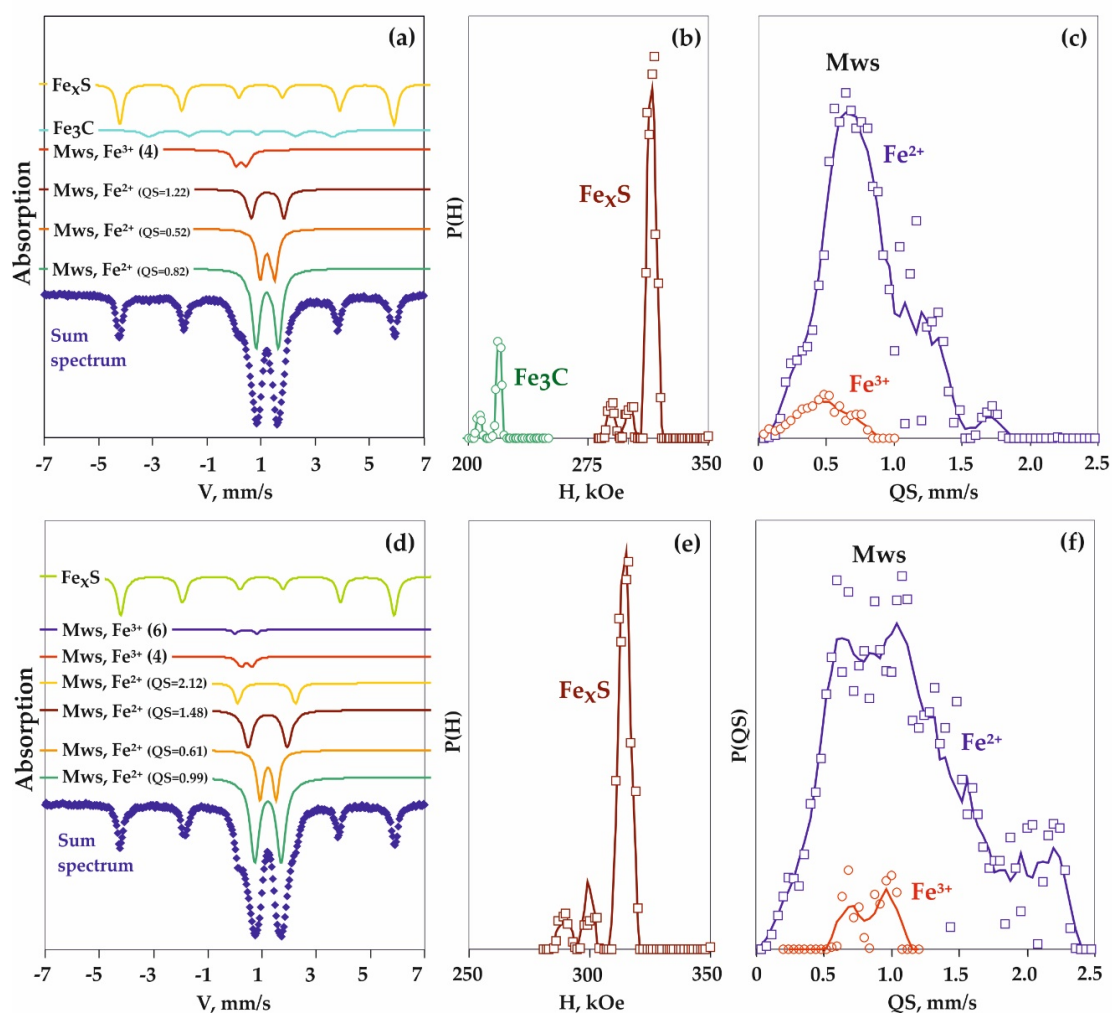


Figure 14. Mössbauer spectra of samples produced in the carbonate-iron-sulphur system (exp. 1623 (a–c) and 1620 (d–f)) as well as components of these spectra (a,d), the probability distribution of hyperfine magnetic fields (H) on iron nuclei (b,e) and the probability distribution of quadrupole splittings $P(QS)$ in experimental spectra of magnesiowüstite and silicates (c,f).

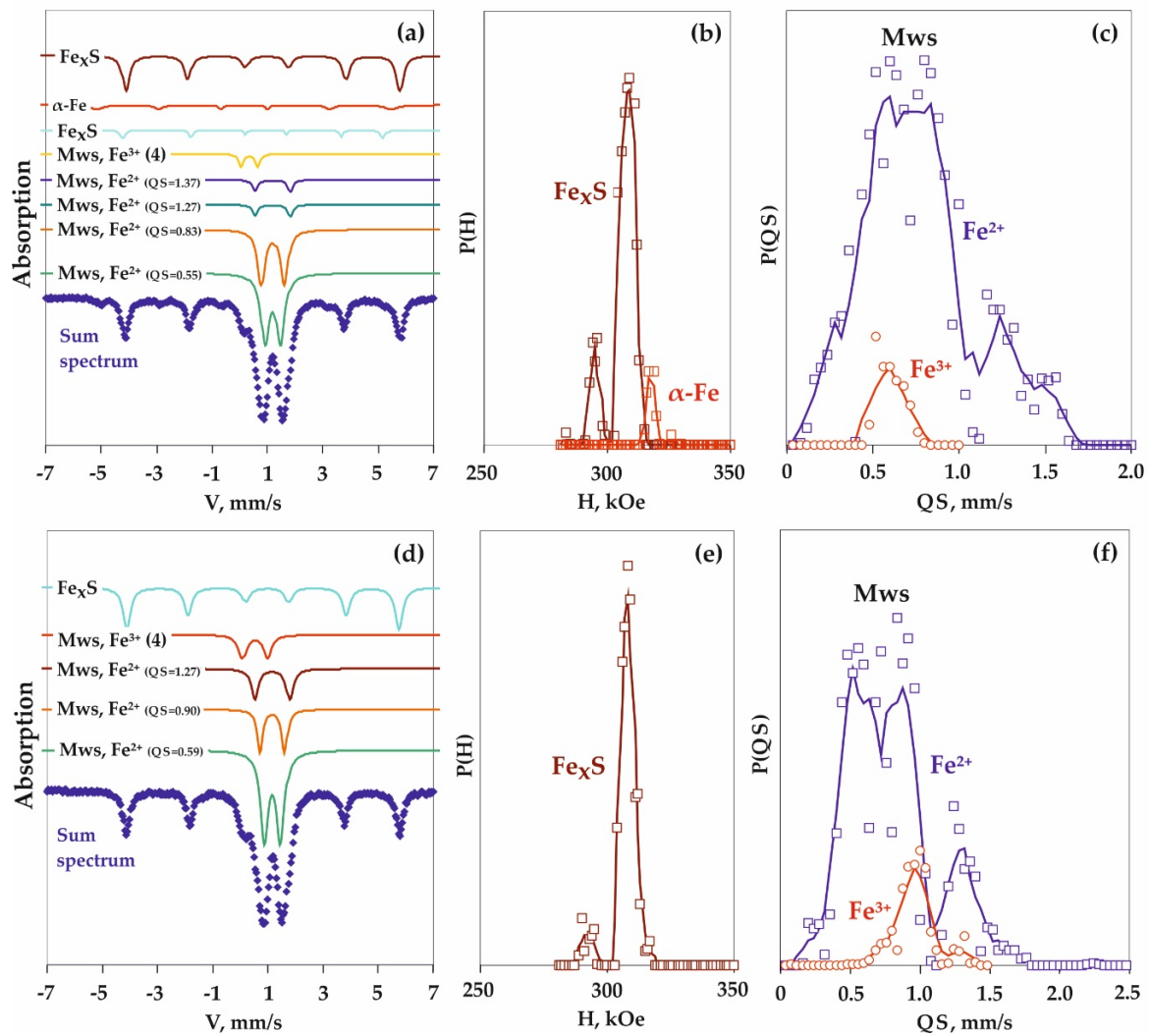
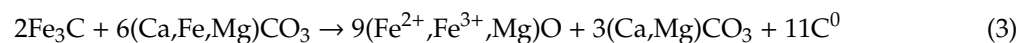


Figure 15. Mössbauer spectra of samples produced in the carbonate-iron system (exp. 1618 (a–c) and 1602 (d–f)) as well as components of these spectra (a,d), the probability distribution of hyperfine magnetic fields (H) on iron nuclei (b,e) and the probability distribution of quadrupole splittings P(QS) in experimental spectra of magnesiowüstite and silicates (c,f).

4. Discussion

4.1. Processes of Fe³⁺-Bearing Magnesiowüstite Formation in the Carbonate-Iron System

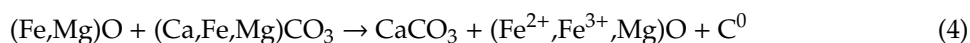
A detailed reconstruction of the interaction processes demonstrates that Fe³⁺-bearing magnesiowüstite in the carbonate-iron system under redox gradient conditions is formed via different scenarios, which occurs in both the reduced and oxidized zones of samples. In the reduced zone (fO_2 values are close to iron-wüstite buffer), magnesiowüstite is a product of iron or iron carbide oxidation upon interaction with carbonate, according to these schematic reactions:



Under these conditions, magnesiowüstite and graphite co-exist mainly with iron carbide. In this case, the Fe³⁺ content in magnesiowüstite is found to be determined by an excess of the oxidizing

agent (carbonate) over the reducing agent (metal or carbide) in Reactions (1) and (3). The formation of magnesiowüstite via a set of reactions is confirmed by the Mössbauer spectroscopy data that demonstrate the concentration heterogeneity of magnesiowüstite, with identification of areas with different contents of magnesium, cationic vacancies and Fe^{3+} .

Magnesiowüstite that is formed in the reduced zone is, in turn, a reducing agent for carbonate ($T \leq 1250$ °C) or a carbonate melt ($T > 1250$ °C) formed in the oxidized zone ($f\text{O}_2$ values are near CCO buffer):



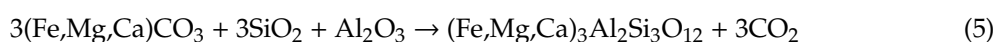
The redox interaction (4) leads to oxidation of magnesiowüstite and an increase in the Fe^{3+} concentration, which is accompanied by reduction of carbonate or a carbonate melt to C^0 (graphite or diamond). Magnesiowüstite produced under these conditions is characterized by different Fe^{3+} concentrations, from moderate to extremely high, which is apparently controlled by the proportions of carbonate and $(\text{Fe,Mg})\text{O}$ in each particular region of the oxidized part in the sample.

It should be noted that an exchange between the reduced center and the oxidized periphery of the reaction volume occurs due to a carbon-bearing fluid or a high calcium carbonate melt capable of dissolving and transporting a significant amount of magnesiowüstite. The solubility of magnesiowüstite in this melt ranges from 15 (1200 °C) to 22 wt.% (1650 °C). Most likely, saturation of the carbonate melt with FeO occurs directly during the redox interaction of the melt with carbide. At the highest temperatures, crystallization of Fe^{3+} -bearing magnesiowüstite occurs due to a combination of processes: (1) dissolution of $(\text{Fe,Mg})\text{O}$ in a high calcium carbonate melt; (2) the redox interaction between a carbonate melt and solid-phase $(\text{Fe}^{2+}, \text{Mg})\text{O}$ with oxidation of dissolved magnesiowüstite and reduction of carbonate to elemental carbon; (3) crystallization of $(\text{Fe}^{2+}, \text{Fe}^{3+}, \text{Mg})\text{O}$, graphite and diamond upon achieving the solubility limit of Fe^{3+} -bearing magnesiowüstite and C^0 in a high calcium carbonate melt. In other words, magnesiowüstite in this case is a sink for ferric iron in a carbonate melt. It is this mechanism that is responsible for formation of the most oxidized magnesiowüstite with extremely high concentrations of ferric iron (up to 34 at.%).

Thus, under redox gradient conditions in the carbonate-iron system, ferric iron concentrations in magnesiowüstite consistently change from 0 in the most reduced regions of samples (IW buffer (about FMQ-5 log units)) to 34 at.% in the most oxidized regions (about FMQ-1 log units). Under these conditions, Fe^{3+} -bearing magnesiowüstite is formed in (a) redox reactions where it is a product of iron or iron carbide oxidation, (b) redox reactions involving magnesiowüstite as a reducing agent for carbonate, (c) processes of magnesiowüstite crystallization from an oxidized Ca-rich carbonate melt (Mws as a sink for ferric iron).

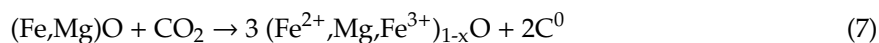
4.2. Processes of Fe^{3+} -Bearing Magnesiowüstite Formation in the Carbonate-Oxide-Metal System

The formation of Fe^{3+} -bearing magnesiowüstite in the carbonate-oxide-metal system under redox gradient conditions was found to occur in both the reduced and oxidized parts of the samples. The formation of magnesiowüstite in an assemblage with carbide in the reduced part of samples ($f\text{O}_2$ values are close to IW buffer) at 1150–1450 °C occurs due to the redox interaction of alkaline earth carbonates and metallic iron according to Reactions (1) and (2). In these reactions, metallic iron is completely converted into carbide that is surrounded by a reaction zone consisting of magnesiowüstite, cohenite and Fe-rich garnet. A small amount of (magnesio)wüstite is formed due to the redox interaction of carbide with CO_2 produced during the decarbonation reaction (5):



Therefore, magnesiowüstite and wüstite formed in Reactions (1), (2) and (6) in the reduced zone of samples are products of carbide oxidation by carbonate or a CO_2 fluid. Further interaction of the

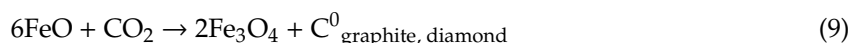
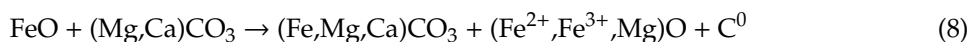
resulting (magnesio)wüstite with a CO₂ fluid leads to reduction of CO₂ to C⁰; some Fe²⁺ in (Fe,Mg)O is oxidized to Fe³⁺, which results in the formation of a Fe³⁺-bearing magnesiowüstite + graphite assemblage in the reduced zone:



Crystallization of a Fe³⁺-magnesiowüstite + graphite + silicate assemblage is observed in the oxidized part of the reaction volume where the redox interaction of Fe²⁺-magnesiowüstite and a CO₂ fluid (7) is considered as the mechanism of Fe³⁺-bearing magnesiowüstite formation. Despite the fact that the phase composition of assemblages produced in the reduced and oxidized parts of samples indicates that the *f*O₂ gradient is present in the reaction volume over an entire temperature range of 1150–1450 °C, Fe³⁺ concentrations in magnesiowüstite are the same throughout the sample. The most likely cause is a sharp difference in the iron content between the reduced center of samples and a more oxidized periphery, which leads to a different intensity of decarbonation reactions with the formation of garnets of different composition, mainly almandine and pyrope garnets, respectively. The difference in the decarbonation intensity and the amount of produced CO₂ fluid is due to the fact that an increase in the iron content shifts the decarbonation curve several hundred degrees to a lower temperature region.

4.3. Processes of Fe³⁺-Bearing Wüstite Formation in the Carbonate-Oxide System

In a range of 1150–1250 °C, the formation of magnesiowüstite in an assemblage with magnetite, graphite and garnet (almandine) at the contact of starting wüstite with an outer carbonate-oxide ampoule occurs during successive reactions of Fe,Mg,Ca-carbonate Formation (8), decarbonation with the formation of Fe-rich garnet and CO₂ (5) and further redox interaction of CO₂ with wüstite (or magnesiowüstite) (7), (9):



Redox interactions (8) and (9) may be considered as reduction of carbonate and CO₂ fluid by magnesiowüstite to elemental carbon (graphite, diamond), which is accompanied by oxidation of magnesiowüstite to (Fe²⁺, Fe³⁺, Mg)O or magnetite. However, it should be noted that these reactions can proceed only at relatively low temperatures and if FeO is present in great excess relative to carbonate and CO₂. Therefore, the formation of an assemblage of Fe³⁺-bearing magnesiowüstite and graphite occurs due to Reactions (7) and (8). At a higher temperature (1350 °C), the degree of decarbonation increases and the processes of garnet and CO₂ fluid formation occur in the entire reaction volume. An increase in the decarbonation degree and amount of CO₂ fluid leads to the fact that the volume of magnetite formed by Reaction (9) exceeds the amount of Fe³⁺-bearing magnesiowüstite. Therefore, we found that the mechanism of Fe³⁺-magnesiowüstite and magnetite formation in the carbonate-oxide system is oxidation of starting wüstite by carbonate or CO₂ fluid and the concentration of ferric iron in magnesiowüstite depends on the degree of system decarbonation.

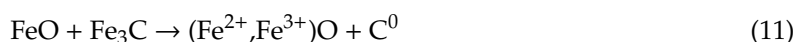
4.4. Processes of Fe³⁺-Bearing Magnesiowüstite Formation in the Carbide-Oxide System

A reconstruction of processes in the cohenite-hematite system demonstrates that wüstite interacts with graphite by redox Reaction (10) that proceeds completely even at a relatively low temperature of 900 °C (*t* = 18 h):

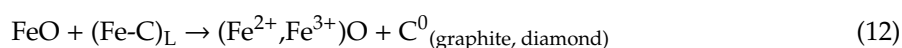


The stoichiometry of this redox reaction excludes a ferric iron impurity in magnesiowüstite. But according to Mössbauer spectroscopy, wüstite produced in this reaction contains 2–4 at.% of Fe³⁺.

This is explained by further interaction of newly formed wüstite with cohenite (small excess of the starting iron carbide was used) in the system. This reaction proceeds through iron disproportionation and leads to crystallization of Fe³⁺-bearing wüstite in equilibrium with graphite:



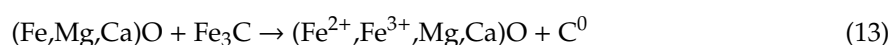
At $T \geq 1400^\circ\text{C}$, the interaction of wüstite with a metal-carbon melt is accompanied by disproportionation of iron, which also leads to the formation of Fe³⁺-bearing wüstite and graphite (\pm diamond growth):



Therefore, it is experimentally demonstrated that the formation of an assemblage of Fe³⁺-bearing wüstite + graphite/diamond under mantle P,T parameters may occur due to iron disproportionation processes during iron carbide + wüstite and metal-carbon melt + wüstite interactions; however, the Fe³⁺ concentration in wüstite produced in this way would not exceed 4 at.%, regardless of temperature.

4.5. Processes of Fe³⁺-Bearing Magnesiowüstite Formation in the Carbonate-Iron-Sulfur System

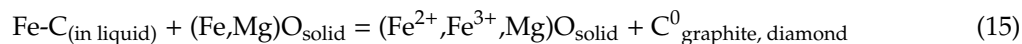
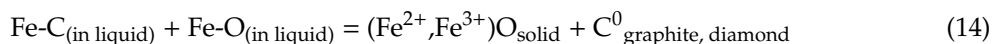
At temperatures of 900 and 1000 °C, the iron-carbonate-sulphur interaction leads to the formation of Fe³⁺-bearing magnesiowüstite in an assemblage with graphite, pyrrhotite, cohenite and \pm Fe,Ca,Mg-carbonate. The main processes that are present in this temperature range and associated with crystallization of Fe³⁺-magnesiowüstite are redox reactions of Mg,Ca-carbonates with iron or iron carbide, which are similar to those described above for the carbonate-metal system (reactions 1–3). The formation of Fe³⁺-magnesiowüstite in an assemblage with graphite can also occur during the redox interaction of magnesiowüstite with cohenite, leading to iron disproportionation:



In a range of 1100–1200 °C, carbonates and iron carbide are completely consumed in Reactions (1–3) and a near-equilibrium assemblage of Fe³⁺-bearing magnesiowüstite + graphite + pyrrhotite is formed. At $T \geq 1300^\circ\text{C}$, interactions in the carbonate-iron-sulphur system lead to crystallization of Fe³⁺-bearing magnesiowüstite and graphite as well as to the formation of two melts, Fe–S–O and Fe–S–C. It is known that at similar P and T, two immiscible melts, Fe–S and Fe–S–C, are formed in the Fe–S–C system [75] and a reduced Fe–C melt and an oxidized carbonate melt are formed in the carbonate-iron system [63]. In a more complex carbonate-iron-sulphur system, the carbonate melt is involved in redox reactions with sulphide and metal-sulphide melts, which results in the formation of Fe–S–O and Fe–S–C melts, as well as crystallization of Fe³⁺-bearing magnesiowüstite and graphite. Below, we present a reconstruction of the Fe³⁺-magnesiowüstite formation involving Fe–S–C and Fe–S–O melts, without focusing on graphite and diamond formation, which was described elsewhere [63,68,75–77].

An analysis of quenching aggregates of melts showed that the carbonate-iron-sulphur interaction results in the generation of two predominantly sulphide melts contrast in $f\text{O}_2$, with one of them being Fe²⁺-bearing (as dissolved FeO) and the other containing metallic iron. We previously demonstrated that the interaction between a metal-carbon melt and wüstite was accompanied by iron disproportionation (reaction 12), which resulted in the formation of a Fe³⁺-bearing magnesiowüstite + graphite/diamond assemblage. Direct evidence of the redox interaction between Fe–S–O and Fe–S–C melts is crystallization of diamond and graphite in the Fe–S–C melt and the formation of Fe²⁺ and Fe³⁺ enriched magnesiowüstite rims at the contact with the Fe–S–O melt. It should be noted that crystallization of Fe³⁺-magnesiowüstite in assemblage with graphite and diamond most likely occurs due to both the redox interaction between melts with involvement of magnesiowüstite, which acts as a

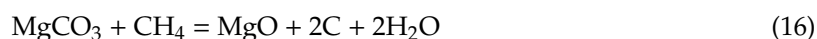
sink for Fe^{3+} and a direct interaction between the Fe–S–C melt and magnesiowüstite, according to the reactions:



Thus, a reconstruction of the carbonate-iron-sulphur interaction revealed that the main mechanism of Fe^{3+} -magnesiowüstite crystallization at $T \leq 1250$ °C is iron and iron carbide oxidation upon their redox interactions with carbonate (Reactions 1–3). At given T, additional scenarios leading to the formation of Fe^{3+} -bearing magnesiowüstite (+graphite) may include the redox interaction between cohenite and magnesiowüstite (reaction 13). At higher temperatures, the formation of Fe^{3+} -bearing magnesiowüstite, graphite and diamond is found to occur due to the redox interaction of Fe–S–O and Fe–S–C melts as well as magnesiowüstite and a Fe–S–C melt.

4.6. Processes of Fe^{3+} -Bearing Magnesiowüstite Formation in the Lithospheric Mantle

Previously, the possibility of (Mg,Fe)O being stable not only in the lower mantle but in the upper mantle were experimentally and theoretically studied in studies [15,16,78]. In particular, Na concentrations in natural ferropericlase in diamond inclusions were experimentally found to be achieved at the upper mantle P,T parameters. Ferropericlase and magnesiowüstite were experimentally demonstrated to be stable in upper mantle domains with low silicon activity. In particular, it is supposed that (Fe,Mg)O is formed in carbonated dunite due to diamond-forming redox reactions between magnesite and reduced fluid:



as well as a concomitant Fe–Mg exchange reaction between olivine and periclase.

In addition to redox reactions, magnesiowüstite (in an assemblage with olivine) is supposed to be capable of crystallizing from a carbonatite melt with very low Si concentrations, which undergoes CO_2 -degassing upon a decrease in pressure. This suggestion was experimentally confirmed in Reference [78] that demonstrated a significant expansion of the ferropericlase crystallization field in carbonate-bearing melts, strongly undersaturated with Si upon a decrease in pressure.

Therefore, both of the previously proposed models for the formation of periclase-wüstite series minerals in the upper mantle suggest involvement of carbonate (as a solid phase or a melt) in them. According to these models, the mechanisms of (Mg,Fe)O crystallization involve reduction of carbonate to $\text{C}^0 + (\text{Mg,Fe})\text{O}$ as well as crystallization of ferropericlase from a carbonate-bearing melt upon a decrease in pressure and a corresponding change in the melt composition — a decrease in CO_2 and silicon concentrations.

Our experimental findings are in good agreement with the results of [14–16] and demonstrate that magnesiowüstite can form in lithospheric mantle rocks via several different scenarios associated with subduction of oxidized crustal carbonate-bearing material to a reduced metal-bearing mantle. Experimental studies have demonstrated that the concentration of metallic iron spread to a metal-saturated mantle (at depths above 250 km) is about 0.1–0.2 wt. % (1400 ppm) [79,80]. In this case, if the mantle is not depleted in carbon (300–800 ppm C), metallic iron is most likely involved in carbides (Fe_3C and Fe_7C_3). Subduction of crustal carbonate-bearing material to mantle depths is known to be a source of mantle metasomatic agents (e.g., C–O–H fluid, carbonate-silicate melts) formed due to decarbonation, dehydration and partial melting of slab rocks. However, some subducted Mg–Ca carbonates can be stable to lower mantle depths (up to 600 km) [58,60,81,82]. Accordingly, in a metal-saturated mantle, redox graphite- and diamond-forming reactions between native iron or iron carbide and solid-phase carbonates or CO_2 dominated fluid or carbonate-bearing melts may occur. Our experiments at pressures characteristic of the metal-precipitation curve demonstrated that

the main product of these reactions, as well as iron disproportionation reactions, was Fe^{3+} -bearing magnesiowüstite in an assemblage with graphite and diamond.

5. Conclusions

We found that under redox gradient in the carbonate-iron system, ferric iron concentrations in magnesiowüstite consistently change from 0–5 at.% in the most reduced sample areas (buffer IW (about FMQ-5 log units)), where magnesiowüstite is in an assemblage with cohenite and graphite/diamond, up to 34 at.% in the most oxidized (about FMQ-1 log units), where magnesiowüstite co-exists with carbonate melt, graphite and diamond. Under these conditions, Fe^{3+} -bearing magnesiowüstite is formed due to (a) redox reactions where it is a product of iron or iron carbide oxidation upon their interaction with carbonate, (b) redox reactions involving magnesiowüstite as a reducing agent for carbonate and (c) magnesiowüstite crystallization from an oxidized high-calcium carbonate melt (Mws as a sink for ferric iron).

Magnesiowüstite that is produced under redox gradient in the carbonate-oxide-metal system in reducing (IW buffer) and oxidizing (about FMQ-1 log units) conditions contains 5–7 at.% of Fe^{3+} . Under reducing conditions, Fe^{2+} -magnesiowüstite is formed by the redox interaction between alkaline-earth carbonates and metallic iron as well as by oxidation of carbide by carbonate or CO_2 fluid. Further interaction of the produced (magnesio)wüstite with CO_2 fluid in reducing and oxidizing conditions leads to reduction of CO_2 to C^0 and formation of the Fe^{3+} -bearing magnesiowüstite + graphite assemblage.

In the carbonate-oxide system, Fe^{3+} -bearing magnesiowüstite was found to be formed only in an assemblage with magnetite, garnet and graphite due to the redox interaction between carbonate or decarbonation-derived CO_2 and starting wüstite. The Fe^{3+} concentrations in synthesized magnesiowüstite (5–12 at.%) and the amount of newly formed magnetite increase as the temperature is elevated and the degree of system decarbonation is correspondingly increased.

The formation of a Fe^{3+} -bearing magnesiowüstite + graphite/diamond assemblage during the carbide-oxide interaction occurs due to iron disproportionation reactions upon iron carbide + wüstite and metal-carbon melt + wüstite interactions; however, the Fe^{3+} concentration in wüstite produced in this way does not exceed 4 at. % and does not depend on temperature.

Upon the iron-carbonate-sulphur interaction at $T \leq 1250$ °C, the main mechanism of Fe^{3+} magnesiowüstite (5–8 at.% of Fe^{3+}) crystallization is iron and iron carbide oxidation in redox interactions with carbonate as well as the redox interaction between cohenite and Fe^{2+} -magnesiowüstite. At $T > 1250$ °C, the formation of Fe^{3+} -bearing magnesiowüstite (9–13 at.% of Fe^{3+}) in an assemblage with graphite or diamond occurs due to redox interactions of Fe–S–O and Fe–S–C melts as well as Fe^{2+} -magnesiowüstite and a Fe–S–C melt. In these processes, Fe^{3+} -bearing magnesiowüstite is not only a product of metal or carbide phase oxidation but also a sink for ferric iron in redox reactions of two $f\text{O}_2$ contrast melts.

Author Contributions: Conceptualization, Y.B. (Yuliya Bataleva) and Y.P.; Data curation, Y.B. (Yuliya Bataleva) and Y.P.; Formal analysis, Y.B. (Yuliya Bataleva) and O.B.; Investigation, Y.B. (Yuliya Bataleva), Y.P., Y.B. (Yuri Borzdov) and O.B.; Methodology, Y.B. (Yuri Borzdov); Visualization, Y.B. (Yuliya Bataleva); Writing—original draft, Y.B. (Yuliya Bataleva); Writing—review & editing, Y.B. (Yuliya Bataleva) and Y.P.

Funding: This research was performed by state assignment of IGM SB RAS (project No. 0330-2016-0007).

Acknowledgments: The authors thank S. Ovchinnikov for his assistance in implementation of the Mössbauer spectroscopy measurements and A. Moskalev for his assistance in the work preparation.

Conflicts of Interest: The authors declare no conflict of interest.

References

1. Irifune, T. Absence of an aluminous phase in the upper part of the Earth's lower mantle. *Nature* **1994**, *370*, 131–133. [[CrossRef](#)]

2. Fei, Y.; Bertka, C.M. Phase transitions in the Earth's mantle and mantle mineralogy. In *Mantle Petrology: Field Observations and High Pressure Experimentation: A Tribute to Francis R. (Joe) Boyd*; Fei, Y., Bertka, C.M., Mysen, B.O., Eds.; Special Publication No. 6; Geochemical Society: Washington, DC, USA, 1999; pp. 189–207.
3. Wood, B.J. Phase transformations and partitioning relations in peridotite under lower mantle conditions. *Earth Planet. Sci. Lett.* **2000**, *174*, 341–354. [[CrossRef](#)]
4. Irifune, T.; Shinmei, T.; McCammon, C.A.; Miyajima, N.; Rubie, D.C.; Frost, D.J. Iron partitioning and density changes of pyrolite in Earth's lower mantle. *Science* **2010**, *327*, 193–195. [[CrossRef](#)] [[PubMed](#)]
5. Ringwood, A.E. Phase transformations and their bearing on the constitution and dynamics of the mantle. *Geochim. Cosmochim. Acta* **1991**, *55*, 2083–2110. [[CrossRef](#)]
6. Fei, Y.; Mao, H.K.; Shu, J.; Hu, J. P-V-T equation of state of magnesiowüstite ($\text{Mg}_{0.6}\text{Fe}_{0.4}\text{O}$). *Phys. Chem. Miner.* **1992**, *18*, 416–422. [[CrossRef](#)]
7. Mao, H.K.; Shu, J.; Fei, Y.; Hu, J.Z.; Hemley, R.J. The wüstite enigma. *Phys. Earth Planet. Int.* **1996**, *96*, 135–145. [[CrossRef](#)]
8. Dubrovinsky, L.S.; Dubrovinskaya, N.A.; Annersten, H.; Hälenius, E.; Harryson, H.; Tutti, F.; Rekhi, S.; LeBihan, T. Stability of ferropericlase in the lower mantle. *Science* **2000**, *289*, 430–432. [[CrossRef](#)]
9. Lin, J.-F.; Heinz, D.L.; Mao, H.K.; Hemley, R.J.; Devine, J.M.; Li, J.; Shen, G. Stability of magnesiowüstite in Earth's lower mantle. *Proc. Natl. Acad. Sci. USA* **2003**, *100*, 4405–4408. [[CrossRef](#)]
10. Kaminsky, F. Mineralogy of the lower mantle: A review of 'super-deep' mineral inclusions in diamond. *Earth Sci. Rev.* **2012**, *110*, 127–147. [[CrossRef](#)]
11. Liu, L.-G. Silicate perovskite from phase transformations of pyrope-garnet at high pressure and temperature. *Geophys. Res. Lett.* **1974**, *1*, 277–280. [[CrossRef](#)]
12. Liu, L.-G. Post oxide phases of forsterite and enstatite. *Geophys. Res. Lett.* **1975**, *2*, 417–419. [[CrossRef](#)]
13. Gurney, J.J. Diamonds. In *Kimberlites and Related Rocks*; Ross, J., Jaques, A.L., Fewson, J., Green, D.H., O'Reilly, S.Y., Danchin, R.V., Janse, A.J.A., Eds.; Special Publication 14; Geological Society of Australia: Carlton, Australia, 1989; Volume 2, pp. 935–965.
14. Bulatov, V.K.; Gurnis, A.V.; Brey, G.P.; Woodland, A.B.; Höfer, H.E. Ferropericlase crystallization under upper mantle conditions. *Contrib. Mineral. Petrol.* **2019**, *174*, 45. [[CrossRef](#)]
15. Stachel, T.; Harris, J.W.; Brey, G.P.; Joswig, W. Kankan diamonds (Guinea): II. Lower mantle inclusion paragenesis. *Contrib. Mineral. Petrol.* **2000**, *140*, 34–47. [[CrossRef](#)]
16. Brey, G.P.; Bulatov, V.; Gurnis, A.; Harris, J.W.; Stachel, T. Ferropericlase—A lower mantle phase in the upper mantle. *Lithos* **2004**, *77*, 655–663. [[CrossRef](#)]
17. Wicks, J.; Duffy, T.S. Crystal structures of minerals in the lower mantle. In *Deep Earth: Physics and Chemistry of the Lower Mantle and Core (Geophysical Monograph Series)*; John Wiley & Sons, Inc. (American Geophysical Union): New York, NY, USA, 2016; pp. 68–88.
18. Kaminsky, F.V. *The Earth's Lower Mantle: Composition and Structure*; Springer: Geneva, Switzerland, 2017; p. 331.
19. Dorfman, S.M.; Shieh, S.R.; Meng, Y.; Prakapenka, V.B.; Duffy, T.S. Synthesis and equation of state of perovskites in the $(\text{Mg,Fe})_3\text{Al}_2\text{Si}_3\text{O}_{12}$ system to 177 GPa. *Earth Planet. Sci. Lett.* **2012**, *357–358*, 194–202. [[CrossRef](#)]
20. Duffy, T.S.; Hemley, R.J.; Mao, H.-K. Equation of state and shear strength at multimegabar pressures: Magnesium oxide to 227 GPa. *Phys. Rev. Lett.* **1995**, *74*, 1371–1375. [[CrossRef](#)]
21. Fei, Y.; Mao, H.K. In situ determination of the NiAs phase of FeO at high pressure and temperature. *Science* **1994**, *266*, 1678–1680. [[CrossRef](#)]
22. Kondo, T.; Ohtani, E.; Hirao, N.; Yagi, T.; Kikegawa, T. Phase transitions of $(\text{Mg,Fe})\text{O}$ at megabar pressures. *Phys. Earth Planet. Int.* **2004**, *143–144*, 201–213. [[CrossRef](#)]
23. Fischer, R.A.; Campbell, A.J. High pressure melting of wüstite. *Am. Miner.* **2010**, *95*, 1473–1477. [[CrossRef](#)]
24. Fischer, R.A.; Campbell, A.J.; Lord, O.T.; Shofner, G.A.; Dera, P.; Prakapenka, V.B. Phase transition and metallization of FeO at high pressures and temperatures. *Geophys. Res. Lett.* **2011**, *38*, L24301. [[CrossRef](#)]
25. Fischer, R.A.; Campbell, A.J.; Shofner, G.A.; Lord, O.T.; Dera, P.; Prakapenka, V.P. Equation of state and phase diagram of FeO. *Earth Planet. Sci. Lett.* **2011**, *304*, 496–502. [[CrossRef](#)]
26. Ozawa, H.; Hirose, K.; Tateno, S.; Sata, N.; Ohishi, Y. Phase transition boundary between B1 and B8 structures of FeO up to 210 GPa. *Phys. Earth Planet. Int.* **2010**, *179*, 157–163. [[CrossRef](#)]

27. Ohta, K.; Fujino, K.; Kuwayama, Y.; Kondo, T.; Shimizu, K.; Ohishi, Y. Highly conductive iron rich (Mg, Fe)O magnesiowüstite and its stability in the Earth's lower mantle. *J. Geophys. Res. Solid Earth* **2014**, *119*, 4656–4665. [[CrossRef](#)]
28. Wicks, J.K.; Jackson, J.M.; Sturhahn, W.; Zhuravlev, K.K.; Tkachev, S.N.; Prakapenka, V.B. Thermal equation of state and stability of (Mg_{0.06}Fe_{0.94})O. *Phys. Earth Planet. Int.* **2015**, *249*, 28–42. [[CrossRef](#)]
29. Katsura, T.; Yoneda, A.; Yamazaki, D.; Yoshino, T.; Ito, E. Adiabatic temperature profile in the mantle. *Phys. Earth Planet. Int.* **2010**, *183*, 212–218. [[CrossRef](#)]
30. Harte, B.; Harris, J.W.; Hutchison, M.T.; Watt, G.R.; Wilding, M.C. Lowermantle mineral associations in diamonds from São-Luiz, Brazil. In *Mantle Petrology: Field Observations and High Pressure Experimentation: A Tribute to Francis R. (Joe) Boyd*; Fei, Y., Bertka, C.M., Mysen, B.O., Eds.; Special Publication No. 6; Geochemical Society: Washington, DC, USA, 1999; pp. 125–153.
31. McCammon, C. Deep diamond mysteries. *Science* **2001**, *293*, 813–814. [[CrossRef](#)]
32. McCammon, C.A.; Stachel, T.; Harris, J.W. Iron oxidation state in lower mantle mineral assemblages: II. Inclusions in diamonds from Kankan, Guinea. *Earth Planet. Sci. Lett.* **2004**, *222*, 423–434. [[CrossRef](#)]
33. Harte, B. Diamond formation in the deep mantle: The record of mineral inclusions and their distribution in relation to mantle dehydration zones. *Mineral. Mag.* **2010**, *74*, 189–215. [[CrossRef](#)]
34. Wirth, R.; Dobrzynetska, L.; Harte, B.; Schreiber, A.; Green, H.W. High-Fe (Mg,Fe)O inclusion in diamond apparently from the lowermost mantle. *Earth Planet. Sci. Lett.* **2014**, *404*, 365–375. [[CrossRef](#)]
35. Svicerio, D.P. Distribution and origin of diamonds in Brazil: An overview. *J. Geodyn.* **1995**, *20*, 493–514. [[CrossRef](#)]
36. McCammon, C.A.; Hutchison, M.; Harris, J. Ferric iron content of mineral inclusions in diamonds from São-Luiz: A view into the lower mantle. *Science* **1997**, *278*, 434–436. [[CrossRef](#)]
37. Harte, B.; Hudson, N.F.C. Mineral associations in diamonds from the lowermost upper mantle and uppermost lower mantle. In *Proceedings of the 10th International Kimberlite Conference, Bangalore, India, 6–11 February 2012*; Geological Society of India: Bangalore, India, 2013; Volume 1, pp. 235–253.
38. Hayman, P.C.; Kopylova, M.G.; Kaminsky, F.Y. Lower mantle diamonds from Rio Soriso (Juina area, Mato Grosso, Brazil). *Contrib. Mineral. Petrol.* **2005**, *149*, 430–445. [[CrossRef](#)]
39. Zedgenizov, D.A.; Kagi, H.; Shatsky, V.S.; Ragozin, A.L. Local variations of carbon isotope composition in diamonds from Sao-Luis (Brazil): Evidence for heterogenous carbon reservoir in sublithospheric mantle. *Chem. Geol.* **2014**, *240*, 114–124. [[CrossRef](#)]
40. Bulanova, G.P. The formation of diamond. *J. Geochem. Explor.* **1995**, *53*, 2–23. [[CrossRef](#)]
41. Stachel, T.; Harris, J.W.; Brey, G.P. Rare and unusual mineral inclusions in diamonds from Mwadui, Tanzania. *Contrib. Mineral. Petrol.* **1998**, *132*, 34–47. [[CrossRef](#)]
42. Kaminsky, F.V.; Wirth, R.; Schreiber, A. A microinclusion of lower-mantle rock and some other lower-mantle inclusions in diamond. *Can. Mineral.* **2015**, *53*, 83–104. [[CrossRef](#)]
43. Fei, Y. *Crystal Chemistry of FeO at High Pressure and Temperature*; Special Publication 5; Geochemical Society: Washington, DC, USA, 1996; pp. 243–254.
44. Jacobsen, S.D.; Reichmann, H.J.; Spetzler, H.; Mackwell, S.J.; Smyth, J.R.; Angel, R.J.; McCammon, C.A. Structure and elasticity of single-crystal (Mg,Fe)O and a new method of generating shear waves for gigahertz ultrasonic interferometry. *J. Geophys. Res.* **2002**, *107*, 5867–5871. [[CrossRef](#)]
45. Nestola, F.; Burnham, A.D.; Peruzza, L.; Tauro, L.; Alvaro, M.; Walter, M.J.; Gunter, M.; Anzolini, C.; Kohn, S.C. Tetragonal almandine-pyrope phase, TAPP: Finally a name for it, the new mineral jeffbenite. *Mineral. Mag.* **2016**, *80*, 1219–1232. [[CrossRef](#)]
46. Longo, M.; McCammon, C.A.; Jacobsen, S.D. Microanalysis of the iron oxidation state in (Mg, Fe)O and application to the study of microscale processes. *Contrib. Mineral. Petrol.* **2011**, *162*, 1249–1257. [[CrossRef](#)]
47. Ringwood, A.E. Composition of core and implications for origin of Earth. *Geochem. J.* **1977**, *11*, 111–135. [[CrossRef](#)]
48. Sherman, D.M. The nature of pressure-induced metallization of FeO and its implications to the core-mantle boundary. *Geophys. Res. Lett.* **1989**, *16*, 515–518. [[CrossRef](#)]
49. McWilliams, R.S.; Spaulding, D.K.; Eggert, J.H.; Celliers, P.M.; Hicks, D.G.; Smith, R.F.; Collins, G.W.; Jeanloz, R. Phase transformations and metallization of magnesium oxide at high pressure and temperature. *Science* **2012**, *338*, 1330–1333. [[CrossRef](#)] [[PubMed](#)]

50. Ohta, K.; Cohen, R.E.; Hirose, K.; Haule, K.; Shimizu, K.; Ohishi, Y. Experimental and theoretical evidence for pressure-induced metallization in FeO with rocksalt-type structure. *Phys. Rev. Lett.* **2012**, *108*, 026403. [[CrossRef](#)] [[PubMed](#)]
51. Tremper, R.T.; Giddings, R.A.; Hodge, J.D.; Gordon, R.S. Creep of polycrystalline MgO–FeO–Fe₂O₃ solid-solutions. *J. Am. Ceram. Soc.* **1974**, *57*, 421–428. [[CrossRef](#)]
52. Wood, B.J.; Nell, J. High-temperature electrical-conductivity of the lower-mantle phase (Mg,Fe)O. *Nature* **1991**, *351*, 309–311. [[CrossRef](#)]
53. Mackwell, S.; Bystricky, M.; Sproni, C. Fe–Mg interdiffusion in (Mg,Fe)O. *Phys. Chem. Mineral.* **2005**, *32*, 418–425. [[CrossRef](#)]
54. Otsuka, K.; Longo, M.; McCammon, C.A.; Karato, S.-I. Ferric iron content of ferropericlasite as a function of composition, oxygen fugacity, temperature and pressure: Implications for redox conditions during diamond formation in the lower mantle. *Earth Planet. Sci. Lett.* **2013**, *365*, 7–16. [[CrossRef](#)]
55. Otsuka, K.; McCammon, C.A.; Karato, S. Tetrahedral occupancy of ferric iron in (Mg,Fe)O: Implications for point defects in the Earth's lower mantle. *Phys. Earth Planet. Int.* **2010**, *180*, 179–188. [[CrossRef](#)]
56. Kaminsky, F.V.; Ryabchikov, I.D.; McCammon, C.A.; Longo, M.; Abakumov, A.M.; Turner, S.; Heidari, H. Oxidation potential in the Earth's lower mantle as recorded by ferropericlasite inclusions in diamond. *Earth Planet. Sci. Lett.* **2015**, *417*, 49–56. [[CrossRef](#)]
57. Biellmann, C.; Gillet, P.; Guyot, F.; Peyronneau, J.; Reynard, B. Experimental evidence for carbonate stability in the Earth's lower mantle. *Earth Planet. Sci. Lett.* **1993**, *118*, 31–41. [[CrossRef](#)]
58. Brenker, F.E.; Vollmer, C.; Vincze, L.; Vekemans, B.; Szymanski, A.; Janssens, K.; Szaloki, I.; Nasdala, L.; Joswig, W.; Kaminsky, F. Carbonates from the lower part of transition zone or even the lower mantle. *Earth Planet. Sci. Lett.* **2007**, *260*, 1–9. [[CrossRef](#)]
59. Stagno, V.; Tange, Y.; Miyajima, N.; McCammon, C.A.; Irifune, T.; Frost, D.G. The stability of magnesite in the transition zone and the lower mantle as function of oxygen fugacity. *Geophys. Res. Lett.* **2011**, *38*. [[CrossRef](#)]
60. Boulard, E.; Gloter, A.; Corgne, A.; Antonangeli, D.; Auzende, A.-L.; Perrillat, J.-P.; Guyot, F.; Fiquet, G. New host for carbon in the deep Earth. *Proc. Natl. Acad. Sci. USA* **2011**, *108*, 5184–5187. [[CrossRef](#)] [[PubMed](#)]
61. Kaminsky, F.V.; Wirth, R.; Schreiber, A. Carbonatitic inclusions in deep mantle diamond from Juina, Brazil: New minerals in the carbonate–halide association. *Can. Mineral.* **2013**, *51*, 447–466. [[CrossRef](#)]
62. Zhang, C.-L.; Li, S.; Wu, T.-H.; Peng, S.-Y. Reduction of carbon dioxide into carbon by the active wüstite and the mechanism of the reaction. *Mater. Chem. Phys.* **1999**, *58*, 139–145. [[CrossRef](#)]
63. Palyanov, Y.N.; Bataleva, Y.V.; Sokol, A.G.; Borzdov, Y.M.; Kupriyanov, I.N.; Reutsky, V.N.; Sobolev, N.V. Mantle–slab interaction and redox mechanism of diamond formation. *Proc. Natl. Acad. Sci. USA* **2013**, *110*, 20408–20413. [[CrossRef](#)] [[PubMed](#)]
64. Bataleva, Y.V.; Palyanov, Y.N.; Sokol, A.G.; Borzdov, Y.M.; Bayukov, O.A. The role of rocks saturated with metallic iron in the formation of ferric carbonate–silicate melts: Experimental modeling under PT-conditions of lithospheric mantle. *Russ. Geol. Geophys.* **2015**, *56*, 143–154. [[CrossRef](#)]
65. Bataleva, Y.V.; Palyanov, Y.N.; Sokol, A.G.; Borzdov, Y.M.; Bayukov, O.A. Wüstite stability in the presence of a CO₂-fluid and a carbonate–silicate melt: Implications for the graphite/diamond formation and generation of Fe-rich mantle metasomatic agents. *Lithos* **2016**, *244*, 20–29. [[CrossRef](#)]
66. Bataleva, Y.V.; Palyanov, Y.N.; Borzdov, Y.M.; Bayukov, O.A.; Sobolev, N.V. Conditions for diamond and graphite formation from iron carbide at the P–T parameters of lithospheric mantle. *Russ. Geol. Geophys.* **2016**, *57*, 176–189. [[CrossRef](#)]
67. Bataleva, Y.V.; Palyanov, Y.N.; Borzdov, Y.M.; Novoselov, I.D.; Bayukov, O.A. An effect of reduced S-rich fluids on diamond formation under mantle–slab interaction. *Lithos* **2019**, *336–337*, 27–39. [[CrossRef](#)]
68. Bataleva, Y.V.; Palyanov, Y.N.; Borzdov, Y.M.; Bayukov, O.A.; Sobolev, N.V. The formation of graphite upon the interaction of subducted carbonates and sulfur with metal-bearing rocks of the lithospheric mantle. *Dokl. Earth Sci.* **2016**, *466*, 88–91. [[CrossRef](#)]
69. Palyanov, Y.N.; Borzdov, Y.M.; Khokhryakov, A.F.; Kupriyanov, I.N.; Sokol, A.G. Effect of nitrogen impurity on diamond crystal growth processes. *Cryst. Growth Des.* **2010**, *10*, 3169–3175. [[CrossRef](#)]
70. Pal'yanov, Y.N.; Sokol, A.G.; Borzdov, Y.M.; Khokhryakov, A.F. Fluid-bearing alkaline carbonate melts as the medium for the formation of diamonds in the Earth's mantle: An experimental study. *Lithos* **2002**, *60*, 145–159. [[CrossRef](#)]

71. Sokol, A.G.; Borzdov, Y.M.; Palyanov, Y.N.; Khokhryakov, A.F. High-temperature calibration of a multi-anvil high pressure apparatus. *High Press. Res.* **2015**, *35*, 139–147. [[CrossRef](#)]
72. Aldon, L.; Jumas, J.-C. Lithium-induced conversion reaction in wüstite Fe_{1-x}O studied by ^{57}Fe Mössbauer spectroscopy. *Solid State Sci.* **2012**, *14*, 354–361. [[CrossRef](#)]
73. Greenwood, N.N.; Howe, A.T. Mössbauer studies of Fe_{1-x}O . Part I. The defect structure of quenched samples. *J. Chem. Soc.* **1972**, *1*, 110–116. [[CrossRef](#)]
74. Manning, P.G.; Jones, W.; Birchall, T. Mössbauer spectral studies of iron-enriched sediments from Hamilton Harbor, Ontario. *Can. Miner.* **1980**, *18*, 291–299.
75. Dasgupta, R.; Buono, A.; Whelan, G.; Walker, D. High-pressure melting relations in Fe–C–S systems: Implications for formation, evolution and structure of metallic cores in planetary bodies. *Geochim. Cosmochim. Acta* **2009**, *73*, 6678–6691. [[CrossRef](#)]
76. Pal'yanov, Y.; Borzdov, Y.; Kupriyanov, I.; Gusev, V.; Khokhryakov, A.; Sokol, A. High-pressure synthesis and characterization of diamond from a sulfur-carbon system. *Diam. Relat. Mater.* **2001**, *10*, 2145–2152.
77. Palyanov, Y.N.; Sokol, A.G.; Khokhryakov, A.F.; Pal'yanova, G.A.; Borzdov, Y.M.; Sobolev, N.V. Diamond and graphite crystallization in COH fluid at P–T parameters of the natural diamond formation. *Dokl. Earth Sci.* **2000**, *375*, 1395–1398.
78. Brey, G.P.; Ryabchikov, I.D. Carbon dioxide in strongly undersaturated melts and origin of kimberlitic magmas. *Neues Jahrb. Mineral. Monatsh.* **1994**, *10*, 449–463.
79. Rohrbach, A.; Ballhaus, C.; Golla-Schindler, U.; Ulmer, P.; Kamenetsky, V.S.; Kuzmin, D.V. Metal saturation in the upper mantle. *Nature* **2007**, *449*, 456–458. [[CrossRef](#)] [[PubMed](#)]
80. Rohrbach, A.; Schmidt, M.W. Redox freezing and melting in the Earth's deep mantle resulting from carbon–Iron redox coupling. *Nature* **2011**, *472*, 209–212. [[CrossRef](#)] [[PubMed](#)]
81. Oganov, A.R.; Hemley, R.J.; Hazen, R.M.; Jones, A.P. Structure, bonding and mineralogy of carbon at extreme conditions. *Rev. Mineral. Geochem.* **2013**, *75*, 47–77. [[CrossRef](#)]
82. Martirosyan, N.S.; Shatskiy, A.; Chanyshv, A.D.; Litasov, K.D.; Podborodnikov, I.V.; Yoshino, T. Effect of water on the magnesite–iron interaction, with implications for the fate of carbonates in the deep mantle. *Lithos* **2019**, *326–327*, 435–445. [[CrossRef](#)]



© 2019 by the authors. Licensee MDPI, Basel, Switzerland. This article is an open access article distributed under the terms and conditions of the Creative Commons Attribution (CC BY) license (<http://creativecommons.org/licenses/by/4.0/>).